UNIVERSIDADE D
COIMBRA

David Willian Massicano

Assessment of the Efficiency of Embedded Walls to Mitigate Ground Deformations Induced by Tunnelling

Dissertation of the Masters in Soil Mechanics and Geotechnical Engineering Supervised by Dr. António Manuel Gonçalves Pedro and by Dr. José Carlos Duarte Grazina and presented to the Department of Civil Engineering of the Faculty of Sciences and Technology of the University of Coimbra

Março de 2020

FCTUC DEPARTAMENTO DE ENGENHARIA CIVIL
FACULDADE DE CIÊNCIAS E TECNOLOGIA
UNIVERSIDADE DE COIMBRA

David Willian Massicano

Assessment of the Efficiency of Embedded Walls to Mitigate Ground Deformations Induced By Tunnelling

Avaliação da eficiência de cortinas para mitigação das deformações no maciço induzidas por túneis

Dissertation of the Masters in Soil Mechanics and Geotechnical Engineering
Supervised by Dr. António Pedro and by Dr. José Grazina

Coimbra, 2020

ACKNOWLEDGEMENTS

I wish to thank first, and foremost God, for helping and giving me the strength to pursuit from the beginning until the end of this journey.

It gives me great pleasure in acknowledging the assistance and encouragement of my Professor and Course coordinator Jorge Almeida e Sousa, who was a terrific professor during all this Master's program. Without his encouragement, enthusiasm, and guidance during his classes, this journey would not be possible to be accomplished.

I wish to express my sincere appreciation to my supervisors, Professor Antonio Pedro and Jose Grazina, that since the beginning of this project were very supportive and demonstrated high knowledge skills that helped me to conclude this project. Their guidance during the whole project was essential to submit this work.

I wish to acknowledge the support of my family, my dad, Antonio; my mom Nilse; my brothers Lucas and Thiago; and my girlfriend, Tatiana. They kept me motivating me, supporting me during the hardships that I went through here in Coimbra. Thus, this work without them would not be possible. I also thank all the friends that I have made here in Coimbra from all the different nationalities; without them, the parties would not be the same.

I would also like to thank all my friends who were part of my journey this whole time, David Martins, Guilherme, Artur C, Arthur P., Filype. They were very supportive throughout this time

I also take this opportunity to express my deep sense of gratitude to all the professors from the University of Coimbra and University of Porto, that dedicated their time to all of the students from my class. Each one of you was wonderful people.

RESUMO

O aumento da população nos grandes centros das cidades resultou em uma maior demanda para os sistemas de trânsito. A utilização de túneis foi mostrado como uma ótima solução para melhorar essa crescente demanda por transporte. No entanto, seu uso pode induzir movimentos significativos na superfície do solo, o que pode danificar estruturas localizadas nas proximidades. Existem várias técnicas desenvolvidas para mitigar a magnitude desses movimentos. O objetivo deste estudo é focar em uma medida de mitigação: o uso de cortinas no solo para um caso de um túnel superficial. Tendo como referência o caso da Secção 63 da Linha Verde da rede do Metro de Lisboa, foram realizadas análises numéricas utilizando o software RS2 v2019, assumindo condições de deformação plana. Um estudo paramétrico foi realizado alterando a localização, profundidade e rigidez da cortina. A influência do fator de alívio do estresse em sua eficiência também foi investigada e discutida. Duas relações sem dimensões (local e global), os parâmetros de eficiência, foram empregados para avaliar o desempenho da cortina. A magnitude do impacto da cortina no suporte do túnel também foi investigada. A capacidade da cortina em modificar os assentamentos na superfície de forma favorável foi observada neste estudo específico. Além disso, foi observado um impacto quase insignificante nas forças que atuam no suporte do túnel.

Palavras chave: movimentos do solo; túneis; cortinas

ABSTRACT

The increase of the population in big city centres resulted in a higher demand for the transit systems. Tunnelling has been shown as a great solution to improve this increasing demand for transportation. However, its use can induce significant movements on the ground surface, which can damage structures located nearby. There are several techniques developed to mitigate the magnitude of these movements. The purpose of this study is to focus on one mitigation measure: the use of embedded walls aside from a shallow tunnel. Having as a reference the case of Section 63 of the Green Line of the Lisbon Metro network, numerical analyses were carried out using RS2 v2019 software assuming plane-strain conditions. A parametric study was performed by changing the location, depth and stiffness of the embedded wall. The influence of the stress relief factor on its efficiency was also investigated and discussed. Two dimensionless ratios (local and global), the efficiency parameters, were employed to evaluate the performance of the embedded wall. The magnitude of the impact of the embedded wall in the tunnel lining was also investigated. The ability of the embedded wall in modifying the settlements on the surface in a favourable way was observed in this specific study. In addition, almost insignificant impact on the forces acting on the lining was observed.

Keywords: Ground movements; tunnelling; embedded walls

TABLE OF CONTENTS

LIST OF FIGURES

1 INTRODUCTION

1.1 Scope of Research

Nowadays, in the technological era, the unavoidable growth of the population in big city centres is a ubiquitous trend that results in a higher demand for transit systems and public services. The reason for this continuous growth is related with the intense urbanisation process, which results in a lack of available land and causes higher traffic rates every year, which in turn affects the infrastructure in the cities, especially in what concerns the transportation of people and goods.

Every year, the increase in traffic rates causes tremendous costs for growing metropolitan areas across the globe. This loss leads to the low productivity of workers stuck in traffic. Therefore, to minimise the impact of this problem, many solutions have been discussed by specialists, which involve increasing the efficiency of transportation, maintaining the life quality of the population and minimum environmental impact. Although it is an immense challenge for this inevitable occupation of the ground surface; tunnelling has been shown as a great solution to minimise the use of the land surface, expanding the capability of mass transportation.

The impact on existing buildings and infrastructure is the biggest challenge during the design of a tunnel in an urban area. Ground movements induced by tunnelling can damage existing structures nearby on the surface. Thus, it is necessary a reliable prediction of the ground movements induced by the tunnel excavation in order to minimise and prevent the impact on them. Furthermore, protective measures can be implemented in order to minimise this impact, especially when tunnelling near important and sensitive buildings.

There are case histories among many others published in the literature about the influence of tunnelling in urban areas, such as the case of the buildings above subway tunnels in Frankfurt Clay (Breth & Chambosse, 1975), the Treasury building (Viggiani & Standing, 2001), the case of the Mansion House in London (Frischmann et al., 1994), the case of The Clock Tower and of the Palace of Westminster presented by Burland et al. (2001), and the case of Structural damage caused to RC buildings by tunnelling work (Yildizlar et al., 2014).

This section presents three cases reported in the literature from the damage induced by tunnelling in urban areas. Three cases were selected in order to illustrate the impact of

unexpected ground movements on the nearby buildings. It is interesting to note that none of the buildings collapsed.

Breth & Chambosse (1975) reported a relevant case study wherein tunnelling caused damage in a building in Frankfurt, Germany. The excavation of a 6.7 m diameter tunnel, with a cover-diameter ratio (C/Dt) of about 1.6, and 10-12 m depth, underneath three buildings, caused significant damage on their structure. One of the buildings made of load-bearing masonry suffered large settlements of up to 150 mm. Figure 1 shows the location of the reported cracks on the eastern part of the building. Cracks between 40 to 60 mm were registered mainly in the connection wall between the building and its annexe. 20 mm cracks were also registered through the vaulted basement.

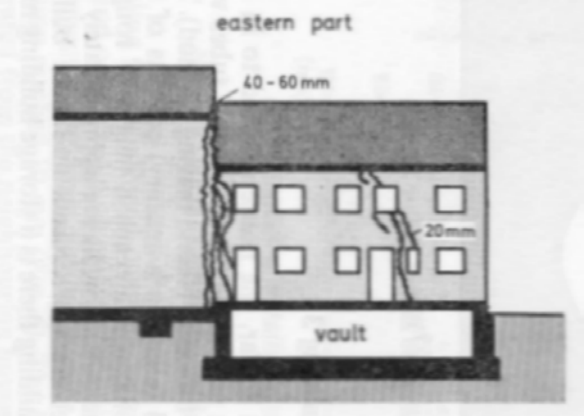

Figure 1- Cracks of masonry building interaction (adapted from Breth and Chambosse, 1975)

In 1995, at London, the construction of the running tunnels for the Jubilee Line Extension (westbound and eastbound) triggered some unexpected volume losses in the Westminster area. At this place, the Treasury Building, which located near to the St. James Park, was affected by these unexpected volumes losses. The westbound and eastbound tunnels had a diameter of 4.85m and were located at 32 m and 23 m depth respectively. The tunnels were excavated in the London Clay formation using a TBM with an open-face and non-pressurized shield. During the design stage, a conservative value of volume loss of about 2% was predicted. However, the measured volume losses were higher than 3% in the Westminster and St. James Park areas.

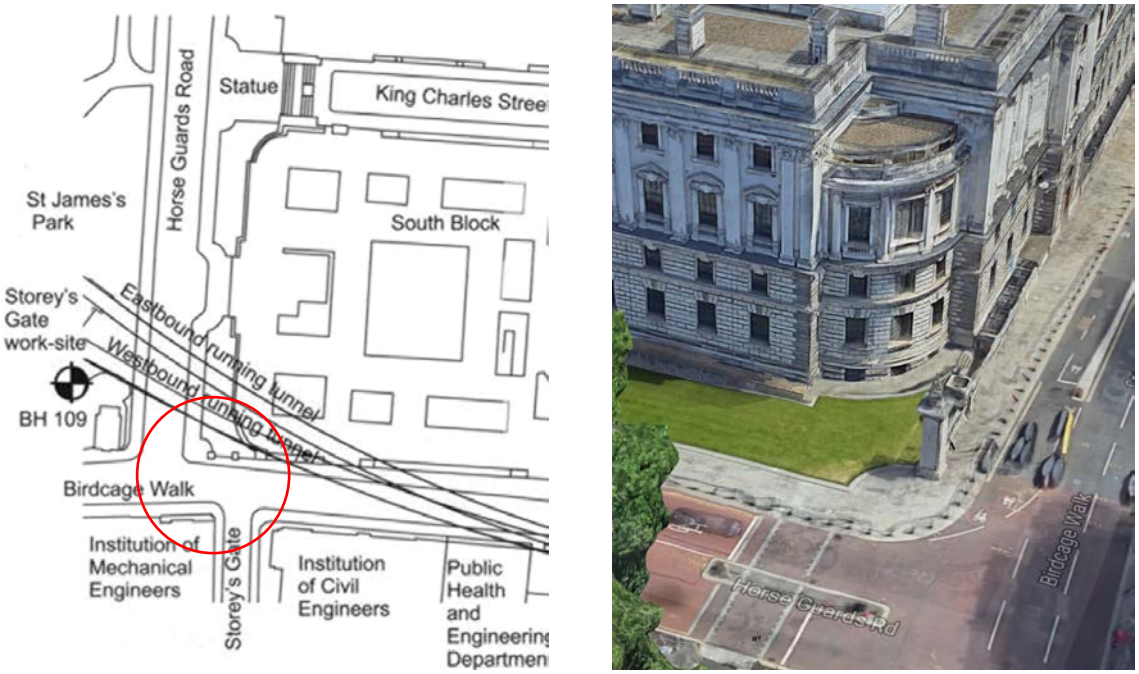

Figure 2- Location of the Treasury building (Viggiani & Standing, 2001).

As a consequence of the unexpected excessive ground volume losses, significant differential settlements on the corner of the building occurred, which were measured by the extensive monitoring at several points of the building. Figure 2 illustrates the location on the corner of House Guards Road and Birdcage Walk street (Viggiani & Standing, 2001). After three months of the excavation of the westbound tunnel, the cumulative settlement of the southwest corner of the building reached nearly 17 mm. The risk of severe damages in the structure was real since the second tunnel excavation was yet to occur. In order to reduce the ongoing settlements, compensation grouting was carried out, reducing any likelihood of damaging the Treasury. In fact, no damages were reported after the excavation works (Viggiani & Standing, 2001).

The last case presented was published by Yildizlar et al. (2014) and occurred in the Istanbul University I.U Cerrapasa Campus in Turkey. The construction of a sewage tunnel with 4.6 m diameter and 22 m depth, triggered significant damages in some Medicine faculty buildings. Figure 3 exhibits the diagonal cracks formed in a wall of the basement floor due to bending (a), shear and compression cracks on a column of one of the faculty buildings (b) and the location of the sewage tunnel axis under the buildings (c). According to Yildizlar et al. (2014), the sudden ground settlements induced during the excavation were responsible for the observed damages. Angular distortions on the beams of more than 1/250 were registered (Yildizlar et al., 2014).

Figure 3- Pictures obtained from the buildings in the Medical Faculty: a) diagonal cracks formed in a wall of the basement floor due to bending; b) shear and compression crack a column of one of the buildings; c) route of the tunnel and location of the buildings highlighted from the Medical Faculty (Yildizlar et al.,2014)

The purpose of this study is to present a numerical analysis of the effects of using an embedded wall on the side of the tunnel in order to mitigate ground movements induced by tunnelling. The investigation presents a bibliography review of case studies where this solution was adopted to protect buildings on the ground surface. Furthermore, this study will focus on evaluating the efficiency of using this protective measure in Section 63 of the Metro Lisbon Network, where significant movements were measured due to the construction of the running tunnel. For that purpose, after proper calibration, a set of numerical analyses were carried out in an attempt to simulate the main aspects of the field problem.

1.2 Thesis Outline

This dissertation incorporates 7 chapters:

Chapter 1 is an introductory chapter that brings attention to the unavoidable growth of traffic rates in city centres. It highlights that tunnelling is a solution in the modern world to expand mass transportation. However, it also describes the consequences of tunnelling in heavily dense areas by describing three case histories. Among these, two of them suffered a visible impact, while the other one mitigation measures were taken in order to protect the structure.

Chapter 2 gives an overview of terms and explanations of general considerations for short-term ground movements for shallow tunnels in soft ground. It depicts two conventional tunnelling methods in urban areas. It reviews the empirical methods from the literature employed to estimate displacements induced by tunnelling. Broadly, this chapter explores some mitigation measures typically taken to mitigate ground movements induced by tunnelling by giving some examples of applications in the past.

Chapter 3 gives a concise bibliography review of studies performed and describes three case histories of using an embedded wall as a mitigation measure of settlements on the ground surface. It also describes in details two reference studies, Bilotta (2008) and Rampello et al. (2019) where this mitigation technique was employed. It explores and discusses the results of centrifuge tests and numerical analyses. Additionally, it describes the use of two dimensionless parameters termed as local and global efficiency to assess the efficacy of the embedded wall in mitigating settlements behind it. The results obtained and the suggestions made from the two studies were discussed and criticized.

Chapter 4 presents the case of study of this dissertation, section 63, which is located between “Cais do Sodré” and “Baixa-Chiado” stations, from the Greenline Lisbon metro network. It briefly describes the background history and reviews with the evolution over time of the metro lines construction. It also describes the construction method employed. The geological and geotechnical conditions from this section are also discussed by describing the instrumentation survey and monitoring plan performed in the field between sections P4 and P13 (instrumented sections within section 63)

Chapter 5 is dedicated to exploring in details the influence of using an embedded wall in the settlement trough by a two-dimensional finite element analysis by using RS2 v2019 software. It describes how the numerical analysis was performed in greenfield, and in the presence of the embedded wall (reference model) for the instrumented section P9. The general conditions of the study, the geometry of the problem, the mesh, the boundary conditions, the constitutive

model, the construction sequence, and the geotechnical parameters adopted also are described. It is included the calibration of the numerical model in order to replicate the instrumented sections P9 and P10A, which involves the stress relief methodology based on the reference results measured in the field. The forces mobilised along the tunnel lining and the embedded wall are also depicted. This chapter also studies the efficiency of the wall by using a local efficiency parameter and describes the implementation of an additional methodology by using a dimensionless parameter that involves assessing the global efficiency of the embedded wall in the settlement trough.

Chapter 6 describes three parametrical studies performed in this investigation by exploring the main factors that could affect the performance of the embedded wall in the problem. In that, sixty-six numerical analyses were computed and it is investigated the influence of the location, depth, and stiffness of the embedded wall on local and global efficiency parameters. In addition to that, the impact of distinct stress relief factor on the efficiency parameters is explored. This chapter also explores and discusses the impact of using an embedded wall in the maximum forces acting along the lining. The forces induced along the embedded wall after the tunnel excavation is also investigated for a better understanding of the soil-structure interaction.

Chapter 7 contains the conclusions and the main findings of the project. It considers how the project carried out varied from the previous studies performed. It also contains recommendations for future research.

2 GENERAL CONCEPTS

2.1 Overview

The key for a successful design of a tunnel relies on three essential factors: stability of the excavation, ground movements and their effects, and performance of the lining (Mair & Taylor, 1997b). This thesis focuses mainly on the ground movements induced by tunnelling and their impact on the ground surface. In tunnels located in a metropolitan area, they are considered the primary concern of tunnel engineers (Chapman et al., 2017). This chapter gives an overview of the typical ground movements induced by tunnelling in the short-term. These movements are closely linked with the type of excavation performed, and therefore a summary of the most employed excavation methods in shallow tunnels is also presented.

Chapman et al. (2017) suggest that tunnelling projects can be classified as either in “soft ground” or “hard rock”. The British Tunnelling Society and the Institution of Civil Engineers in the United Kingdom (Telford, 2004) suggest in their tunnel lining design guide that “soft ground” falls into the category of weak mudstones, weak rocks which include poorer grade chalk, and weakly and/or highly fractured sandstone. The term “hard ground” falls into all the other forms of rock. According to Chapman et al. (2017), in the case of tunnelling in “soft ground” with a low cover-diameter ratio (C/D<2.0), the tunnel crown is assumed to have no bearing capacity, and the groundmass requires immediate support after the excavation. Hence, when tunnelling under these ground conditions, the induced movements on the surface may cause a substantial impact on existing buildings nearby (Chapman et al., 2017).

In general, the primary concerns of tunnel designers are the lining loads, and ground movements induced by tunnelling (Su & Thomas, 2015). According to Simons & Som (1970), 60% of the ground movements occur in the short term, for a typical site in stiff clays. In the long term, according to Attwell & Selby (1989), the settlement trough tends to become more extensive and, although a bigger area is affected, the differential settlements remain similar or even decrease causing equal or less damage on the nearby structures.

2.2 Short-term Ground Movements

Regardless of the tunnelling method, it is impossible to excavate a tunnel and install the lining immediately after creating the void. Stress relief of the ground around the tunnel occurs during the excavation, inducing radial displacements towards the tunnel and axial displacements towards the face. As a result, a void appears at the ground surface, which is usually termed as "settlement trough". The additional ground volume excavated in excess, which is the sum of the radial and face volume loss, gives the total over excavated volume, known as "Volume Loss" or "Ground Loss", V' (Chapman et al., 2017).

The precise estimation of the settlement trough and the total volume loss is a challenging task for tunnel engineers as it depends on different factors, but mainly of the tunnelling method and the ground conditions. The volume loss of the tunnels is often considered as the volume of the settlement trough in the short term (undrained conditions). To simplify the comprehension of the volume loss, V', it is usually expressed as a percentage of the theoretical volume excavated Va.

Figure 4 illustrates the volume of the settlement trough (brown colour) and the coordinate system adopted throughout this thesis, showing a three-dimensional scheme of the ground movements that occur during tunnelling. The coordinate system for this work presents three-axis, where: x denotes a relative distance in the transverse direction for a given section of study; y is the longitudinal direction; z denotes the depth beneath the soil surface. The variable δ_{vmax} located above the tunnel axis represents the maximum settlement of the ground surface, which is obtained after tunnel excavation of a reference section and the induced movements have stabilised.

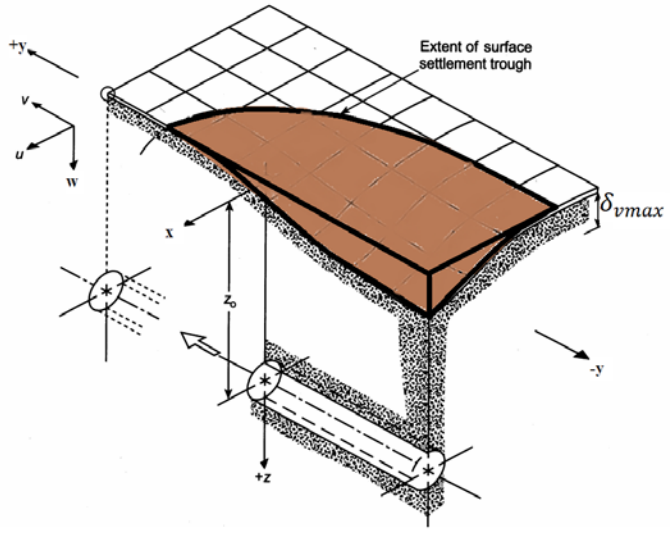

Figure 4-A three-dimensional scheme of the ground movements induced by tunnelling (adapted from Attwell et al., 1986).

2.3 Tunnelling Excavation Methods

The choice of the method of tunnelling excavation plays an essential role in shallow underground construction due to its influence on the ground deformations. Different techniques, in terms of open face and closed face, can be used to bore a tunnel section in soft ground. This section briefly summarises the two commonly employed methods for tunnelling in urban areas. These are, the New Austrian Tunneling Method (NATM) as an open face tunnelling method, and the tunnelling shield closed face method which requires the use of a Tunnel Boring Machine (TBM). Both methods and techniques discussed hold limitations and advantages.

The NATM was developed between 1957 and 1965, and it is still popularly employed around the globe in underground construction. This tunnelling method, which is, in fact, a set of principles, was derived in Austria, during the construction of the Katschberg tunnel (Figure 5). The fundamental idea of this open face methodology is to use the neighbouring groundmass to support the excavation itself with the mobilisation of the strength of soil mass. Consequently, this method is more commonly employed in hard ground. However, it can be employed in the soft ground by using sprayed concrete to support the tunnel immediately after the excavation. As shown in Figure 5, it is commonly employed the adoption of sequential excavation of the section in different stages, which is also a trademark of NATM. With these measures, the ground decompression and strength reduction are minimized during and after the excavation (Chapman et al., 2017).

There are remarkable advantages of using NATM principles. These include geometry flexibility, a small investment in equipment, low-cost labour, and easy access to the tunnel face. On the other hand, the main disadvantage of this method is the significant amount of ground deformations required to mobilise the soil strength, as the stress changes in the surrounding groundmass cause significant ground relaxation. Hence, these changes induce settlements on the ground surface (Chapman et al., 2017).

Figure 5- Excavation of the Katschberg Tunnel crown using NATM (Chapman et al., 2017).

The second excavation method, also known as mechanical tunnelling, is performed by using a TBM. This method excavates using a circular cross-section machine that can bore through almost any type of soil and has the advantage of providing stability to the face excavation and surrounding soil. The application of face pressure allows more precise control of the induced ground movements in the soft ground during the excavation.

There are basically two main types of soft ground TBMs, which are characterized by having a closed face (Chapman et al., 2017):

- Slurry Shield (SS): uses basically a pressurized slurry fluid that applies hydrostatic pressure at the excavation face. It is usually recommended for use in the coarse-grained (cohesionless) ground.

- Earth Pressure Balance (EPB): uses the excavated material to support the tunnel face during the excavation. The ideal soil material for EPB-TBM is fine-grained (cohesive); however, it can be used in coarse-grained materials by "conditioning" the material excavated by using additives such as polymers, foam, and bentonite.

Figure 6 shows an example of an EPB machine used for constructing the Greenline tunnel of the Lisbon Metro network in 1994 (Amaral, 2006). The main advantage of using this tunnelling method, for this case, is the control of the face pressure which can reduce the impact on the ground surface significantly. However, its use has a high upfront cost (Chapman et al., 2017).

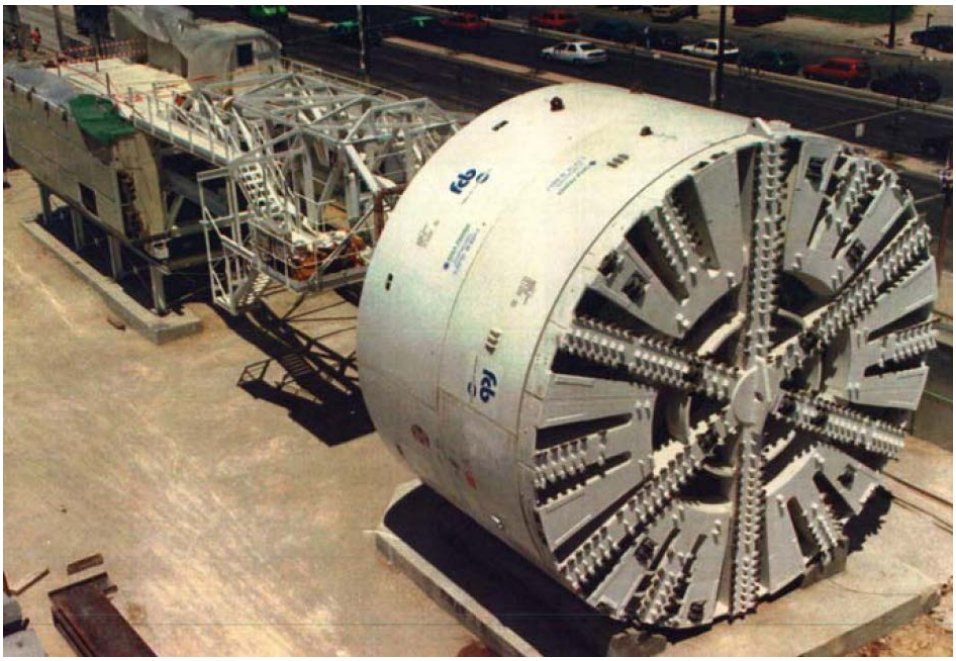

Figure 6- Picture of the EPB-TBM (closed face) used in section 64 of the Lisbon metro network (Amaral, 2006).

2.4 Estimating Displacements Induced by Tunnelling

In 1969, Ralph Peck, based on observation results, verified that a Gaussian distribution could represent the transverse settlement trough induced by the construction of a single tunnel. The Civil Engineering community has widely accepted this suggestion since it fitted a large number of site measurements. Figure 7 illustrates cases of field measurements in three different instrumented sites (Crossrail TBM 1 West Bound-Hyde Park, Jubilee Line Extension West Bound-St. Jame's Park, Channel Tunnel Rail Link up-line, Dagenham) in London and the Gaussian approximation curve. In the figure, the vertical axis denotes the normalized surface settlements and the horizontal axis the normalised transverse offset distance from the tunnel axis (Wan et al., 2016). As can be observed in Figure 7, the Gaussian distribution apparently shows as a good approximation to the field measurements in all the three instrumented sites.

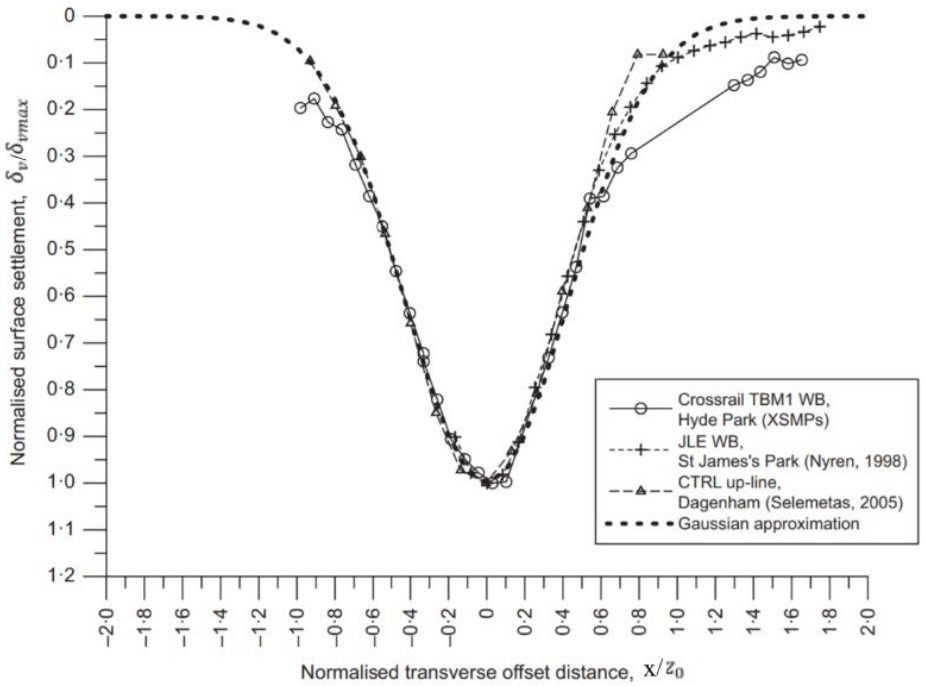

Figure 7- Transverse settlement induced by tunnelling measured in three instrumented sites in London and the Gaussian approximation (Wan et al., 2016).

Figure 8 displays the Gaussian approximation, which is determined using equation 2.1. In that, δ_{vmax} is the maximum settlement at the axis of the tunnel for a given volume loss V', the "x" is the distance at ground surface measured from the centreline of the tunnel, and "i" is the trough width factor that represents the point of inflexion of the curve. This point corresponds to the maximum slope of the Gaussian curve and divides the hogging from the sagging zone. It is noteworthy that the location of the point of inflexion is critical to define the building deformation criteria for risk assessment. In order to define the value of the trough width factor "i", O'Reilly & New (1982) proposed equation 2.2, where this factor is a function of the depth (z), and of the dimensionless trough width parameter (K). The parameter K typically ranges from 0.25 and 0.35 for granular soils (Mair & Taylor, 1996), while cohesive materials often assume values ranging from 0.4 and 0.6 (Mair & Taylor, 1997a).

$$\delta_v(x) = \delta_{vmax} \times \exp\left(-\frac{x^2}{2i^2}\right) \tag{2.1}$$

$$i = K * z \tag{2.2}$$

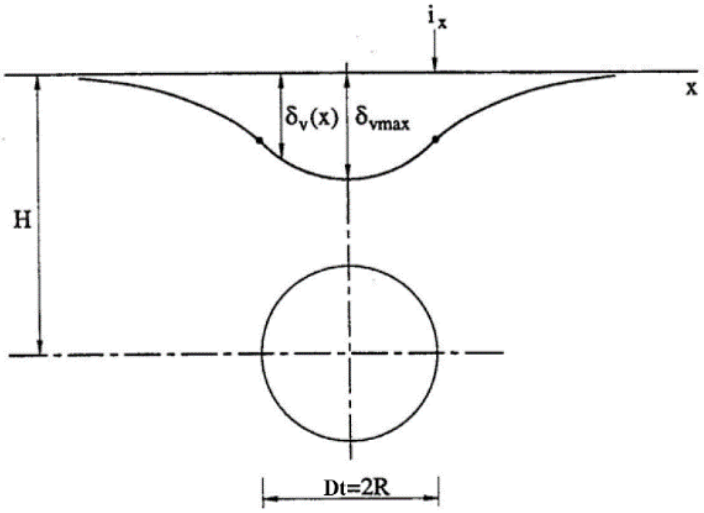

Figure 8- Settlement trough defined by a Gauss distribution (adapted from Almeida e Sousa, 2019).

The area enclosed by the Gaussian curve is expressed by equation 2.3 where the "Volume of the Settlement Trough" is V_{st}, per unit length.

$$V_{st} = \int \delta_v(x) \cdot \mathrm{dx} = \sqrt{2 \cdot \pi} \cdot i_x \cdot \delta_{vmax} \tag{2.3}$$

For the particular cases of the tunnels excavated in Lisbon, the volume of the settlement trough expressed as a percentage of the theoretical volume excavated V_a(equation 2.4), varied from:

$$Va = \frac{\int \delta_v(x) \cdot \mathrm{dx}}{\frac{\pi \cdot Dt^2}{4}} \times 100\ (\%) \tag{2.4}$$

- $0.5 < V_a < 1\%$ for NATM (Amaral, 2006).
- $0.5 < V_a < 1\%$ in soft clays and sands, and between $0.2 < V_a <$ 0.5% in stiff clays or residual soils for closed face TBM (Amaral, 2006).

Another parameter responsible for building damage is the horizontal tensile strain. O'Reilly & New (1982) proposed equation 2.5 to estimate the horizontal ground surface displacement by assuming a simplification that the vectors of the ground movement are directed towards the tunnel axis. In that, H is the depth of the centre of the tunnel.

$$\delta_h(x) = \frac{x.\delta_v(x)}{H} \tag{2.5}$$

By deriving equation 2.5 in order to x, the horizontal strain in the transverse direction of the ground surface can be obtained (equation 2.5).

$$\varepsilon_h(x) = \frac{d\delta_h(x)}{\mathrm{dx}} = \frac{1}{H} \cdot \left(1 - \frac{x^2}{i_x}\right) \cdot \delta_v(x) \tag{2.6}$$

The sign convention of the horizontal strains adopted throughout this thesis is that a negative value represents compression, while a positive value represents tension.

Figure 9 illustrates a cross-section of the transverse horizontal displacements and associated strains on the ground surface induced by tunnelling. The maximum horizontal displacement occurs at the point of inflexion, and the compression strains are located in the zone between the inflexion points (sagging zone). In contrast, tensile strains are developed in the remaining zones (hogging zone).

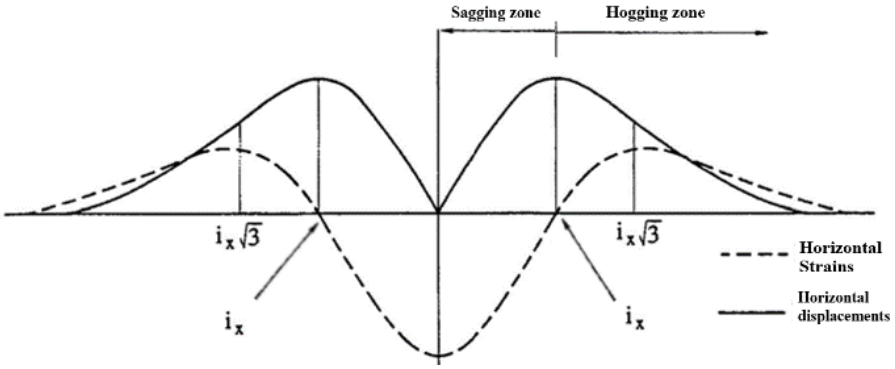

Figure 9- Horizontal displacements and associated strains (adapted from Almeida e Sousa, 2019).

This work only focuses on transversal displacements. However, it is interesting to note that as the tunnel advances in the longitudinal section, displacements at the tunnel face towards its excavation and that propagate up to the ground surface will also occur. Still, tunnel designers usually consider this correspond to a temporary problem since the buildings located ahead of the tunnel face, after initially tilting towards the tunnel face, tend to tilt in the opposite direction once the tunnel excavation moves away, resulting in an almost uniform settlement in the long term.

2.5 Mitigation Measures Typically Adopted

In order to reduce volume loss, Burland (1995) suggested that primarily protective measures within the tunnel should be applied before implementing any ground surface actions. Measures

within the tunnel may include for example but not limited to: the strengthening of the support at or near the face; speed up the application of the support; using Sprayed Concrete Linings; the excavation of the section in smaller sections. These measures tackle the cause of the problem directly, decreasing the soil decompression and are generally less expensive than other measures.

In the case of buildings that require specific protection, due to their position in relation to the tunnel, Burland (1995) suggested the use of other alternative protection measures, such as the described below:

- **Strengthening of the ground:** this technique aims to reduce ground loss by increasing the mechanical properties of the soil at the face of the tunnel (Figure 10a)) or underneath the foundation with grout injections. It allows a safe excavation in case the stability of the tunnel is not sufficient (Almeida e Sousa, 2019). This technique was used in Frankfurter Kreuz Tunnel (Quick et al., 2001), where a 10 m diameter tunnel with a cover of 10 m was excavated in a granular soil just beneath an existing highway. In general, jet grouting columns can be applied isolated, overlapping, or tangent inside the tunnel. Figure 10b) displays the longitudinal section of the Frankfurter Kreuz tunnel with jet grout face columns and roof cover reinforcing the ground. In this case, the adoption of staged excavation protected by jet grout columns reduced the ground movements notably.

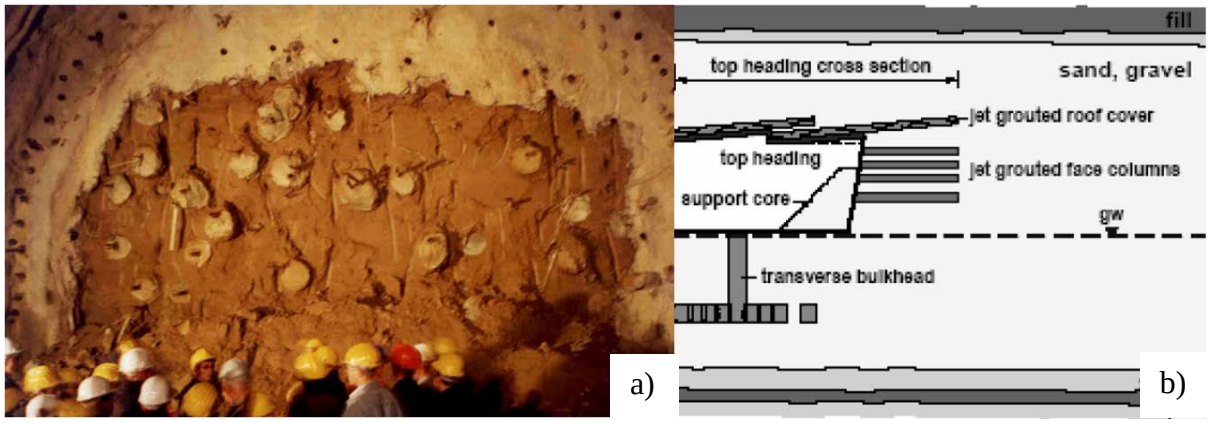

Figure 10- a) Example of jet grouted face columns; b) scheme of the construction details of the Frankfurter Kreuz tunnel(Almeida e Sousa, 2019; Quick et al., 2001).

- **Compensation grouting:** The use of compensation grouting counteracts the movements that occur due to tunnelling. The principle of the technique is to inject grout between the building's foundation and the tunnel to compensate for the ground movement induced by tunnelling (Mair et al., 1994). Figure 11 illustrates an array of grout tubes injected from a shaft (located in the middle of Bridge Street) during the

construction the Jubilee Line Extension Project, which was used to protect the Big Ben from tilting more than the acceptable amount (Harris et al., 1999). The size of the circles represents the quantity of grout injected.

Figure 11- Top view of compensation grouting carried out underneath Big Ben during the construction of the Jubilee Line Extension (Harris et al., 1999).

- **Physical Barrier:** The installation of a physical barrier between the tunnel and the building may be capable of changing the shape of the settlement trough by reducing the settlements behind the wall, and consequently reducing the category of damage of buildings nearby, as alleged Di Mariano et al. (2007). During the excavation of the 12m diameter tunnel for the Metro line in Barcelona at St. Adria street, this protective measure was adopted to protect a 7-storey building located 17m away from the tunnel axis. The scheme of a discontinuous embedded wall (bored pile) construction is illustrated in Figure 12. The excavation was performed in alluvial soil, and a continuous wall of a 65mm diameter of bored piles spacing around two diameters was installed 29.3m depth between the tunnel and the residential building. According to Di Mariano et al. (2007), based on numerical analyses and instrumented results, the category of damage of the building 17m from the tunnel was reduced from 3 to 0.

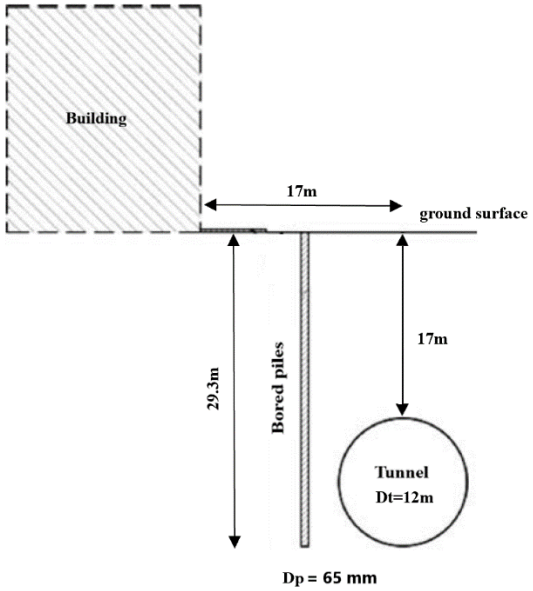

Figure 12- Representation of a discontinuous embedded wall adopted in Metro Line of Barcelona (adapted from Di Mariano et al., 2007)

3 EMBEDDED WALLS AS A MITIGATION MEASURE FOR TUNNELLING

3.1 Background

The design of embedded walls as a mitigation measure for tunnelling is often based on empiricism, rather than based on a rational design process (Rampello et al., 2019). The use of continuous bored piles as the embedded wall was reported from case studies by some authors such as Chen et al. (1998), Di Mariano et al. (2007), Katzenbach et al. (2013), Bai et al., 2014, and Ledesma Villalba & Alonso Pérez de Agreda (2017). It was also reported the use of jet-grouting columns by Sola et al. (2003), Di Mariano et al. (2007), Oteo et al. (2007), and the use of micropiles by Nikiforova & Vnukov (2012). All the reported cases concluded that the use of an embedded wall reduced the ground movements on the footprints of the buildings and, consequently, the potential damage on them (Rampello et al., 2019).

Figure 13 illustrates the first documented case using this mitigation method which occurred at Shangai, during the excavation of the Yan An Dong Lu tunnel (Chen et al., 1998). The ancient astronomical observatory building with 50 m height, required a protective measure due to its proximity from the tunnel excavation. The tunnel had 11 m diameter, axis depth of 28 m and its centerline was located about 15 m distant from the building.

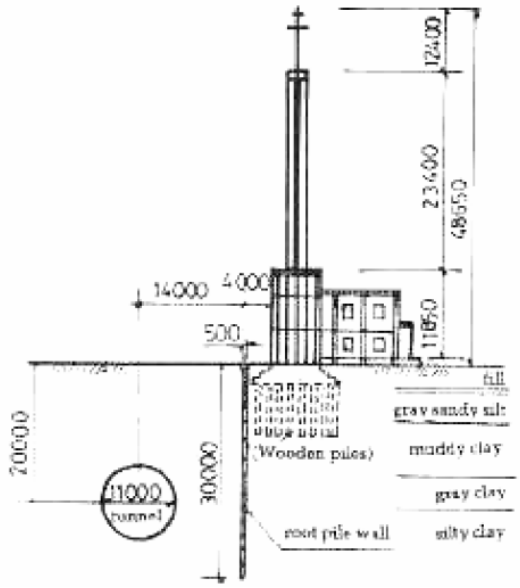

Figure 13- Root piles protecting the Shangai observatory (Chen et al., 1998).

The root piles have 20 cm diameter and were embedded up to about 30 m depth. The line of piles was constructed 14 m away from the tunnel centerline and capped by a reinforced concrete beam, with a length of 14 m. The evaluation of the building tilt after the passage of the tunnel without the pile's protection was predicted to range between 1/200 and 1/100. However, with the use of the root pile wall, the structural tilt measured was reduced to less than 1/1000.

Sola et al. (2003) also reported an embedded wall made of jet-grouting columns to protect a 5-storey building near the construction of a shallow tunnel excavated in soft alluvial soil in Madrid, Spain. The tunnel has a 10 m diameter and 8 m cover. Figure 14 illustrates the discontinuous jet-grouting columns that were constructed between the tunnel and the building. The columns with 1.25 m spacing, started at a depth of 3.6 m and were constructed with an inclination of 17 º, reaching a depth about midway between the tunnel invert and axis. As a result, the ground movements were less than 2 mm in the treated zones, while settlements up to 12 mm were obtained in the untreated zones.

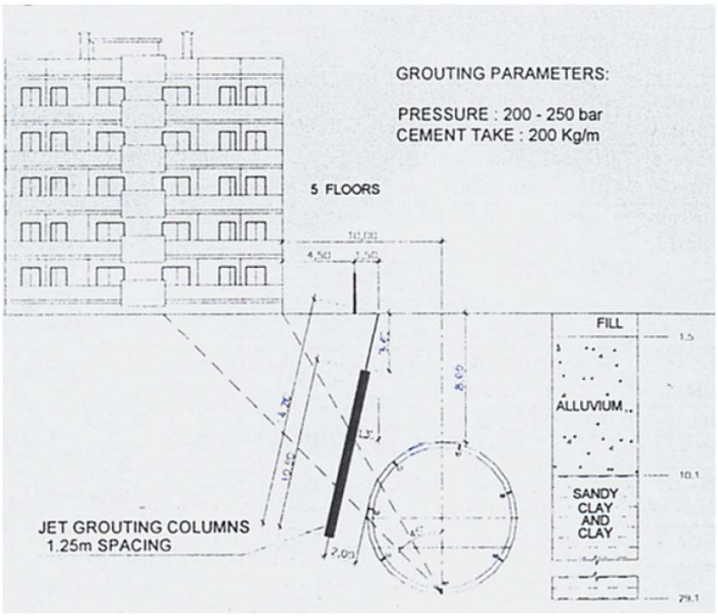

Figure 14- 5-storey building protected by jet-grouting treatment in Madrid, Spain (after Sola et al., 2003)

One of the most recent cases where this mitigation measure was employed was in Barcelona, during the construction of the tunnel that connects the Sants and the Sagrera stations for the high-speed Madrid-Barcelona-France railway. The World Heritage buildings, Casa de Mila and the Sagrada Familia Basilica required protection because of their proximity to the tunnel excavation. The tunnel has 11.5 m diameter and is 25 m deep, crossing the stiff Pliocene substratum (sandy clay and clayey sand). Figure 15 illustrates the ground cross-section showing the embedded row of piles placed between the tunnel and the building. They have 1.5 m diameter, 42 m long and are spaced every 2 m in a total distance of 230 m in the longitudinal plane, before and after the building. Additionally, a reinforced concrete beam capping the pile heads was used to reinforce the connection between them (Ledesma Villalba & Alonso Pérez de Agreda, 2017). The authors alleged based on the instrumentation results and numerical study that the use of the pile wall reduced the settlement by a factor of two in the Sagrada Familia basilica. In contrast to the severe damage predictions, the impact of the tunnel was negligible due to the implementation of this protective measure.

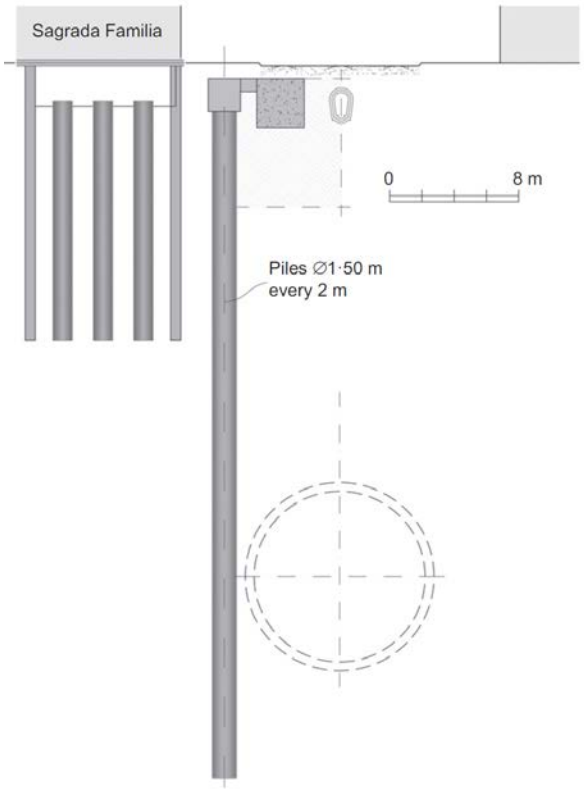

Figure 15- Sagrada Familia basilica being protected by a row of piles between the tunnel and its foundation (Ledesma Villalba & Alonso Pérez de Agreda, 2017).

3.2 Reference studies

In addition to those case studies, Bilotta & Taylor, 2005 and Bilotta (2008) performed centrifuge tests on physical models, in order to evaluate the effectiveness of embedded walls in minimizing the damage in buildings induced by excavating a shallow tunnel in close proximity.

The studies performed by Bilotta (2008) and by Rampello et al. (2019) can be considered as references in this topic since they present a complete literature review supported by experimental and numerical results that explain in detail the interaction between the embedded wall and the soil. Besides numerical analyses, Bilotta (2008) also carried out centrifuge experiments. Rampello et al. (2019) only performed numerical analyses but simulated the effect of employing a discontinuous embedded wall of piles and explored the effects of diaphragm walls installation. In the following sections, the works of these two authors are presented in detail.

3.2.1 Bilotta (2008)

Bilotta (2008) investigated the potential of an embedded diaphragm wall in soft soil in modifying the displacement field induced by tunnelling under greenfield conditions, i.e. without modelling the buildings. Experimental centrifuge tests and a series of numerical analysis were carried out to simulate this interaction with shallow tunnel construction. He also defined an efficiency parameter to quantify the ability of the wall to modify the ground movements. However, it is noteworthy that Billota (2008) neglected the effects of the wall installation in both the numerical analyses and centrifuge tests.

The centrifuge experiment simulated the excavation of an 8m tunnel diameter with C/Dt=1. The diaphragm wall was embedded on one side of the tunnel. Figure 16 depicts the geometry of the experimental model, where C is the tunnel cover, Dt is the tunnel diameter, d the offset from the tunnel axis, L the embedded wall height, and t the wall thickness. The embedded wall height was set at two values 1.5C and 2.5C, corresponding to a short and to a long wall, respectively. The range of the flexural stiffness lied within very flexible (t=0.8 mm) and nearly rigid (t=9.8mm). The offset d was either 1Dt or 1.5Dt. Both rough and smooth wall surfaces were considered in the experiments (Bilotta, 2008).

A slurry of speswhite kaolin was used in the models, while the diaphragm wall was made of aluminium. In order to simulate the stress relief during the excavation the air pressure of the cavity was diminished ($\Delta\sigma_T/Po$), where $\Delta\sigma_T$ change in supporting pressure and Po is the initial soil pressure (Bilotta, 2008).

Simulating the same conditions (shape and size) from the centrifuge model, the numerical analysis was carried out using Sage Crisp (Britto & Gunn, 1987). The soil was modelled using a three-surface kinematic hardening model (Stallebrass, 1990).

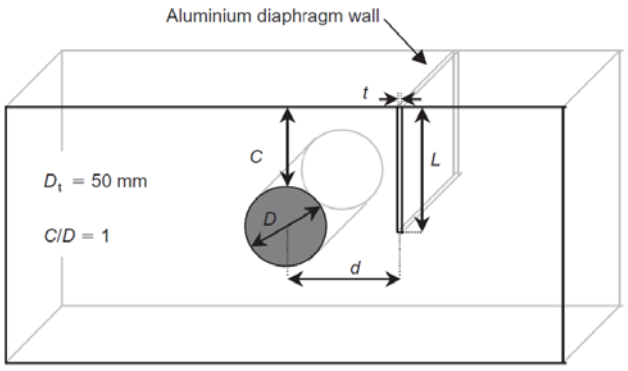

Figure 16- Model geometry used in the centrifuge tests (adapted from Bilotta, 2008).

In order to determine the diaphragm wall's efficiency in reducing the settlements behind the wall, Bilotta, 2008 suggested a dimensionless ratio, η_{bw}^{v}, given by equation 3.1, and determined using the setlements as defined in Figure 17. In the equation, δ_{ref} is the reference settlement under greenfield conditions, without a wall, δ_{bw} is the ground settlement immediately behind the wall, and δ_{w} is the settlement on the top of the wall. In case of a rough interface, δ_{w} it may be equal to the maximum settlement behind the wall, δ_{bw}.

$$\eta_{bw}^{v} = \frac{\delta_{ref} - \delta_{bw}}{\delta_{ref}} \tag{3.1}$$

When $\eta_{bw}^{v} = 1$, the embedded diaphragm wall is entirely effective in reducing settlements behind the wall, since $\delta_{bw} = 0$. On the other hand, the embedded diaphragm wall is considered utterly ineffective if $\eta_{bw}^{v} = 0$, as $\delta_{bw} = \delta_{ref}$. In the case of $\eta_{bw}^{v} < 0$ the effect of the embedded diaphragm wall is detrimental (Bilotta, 2008).

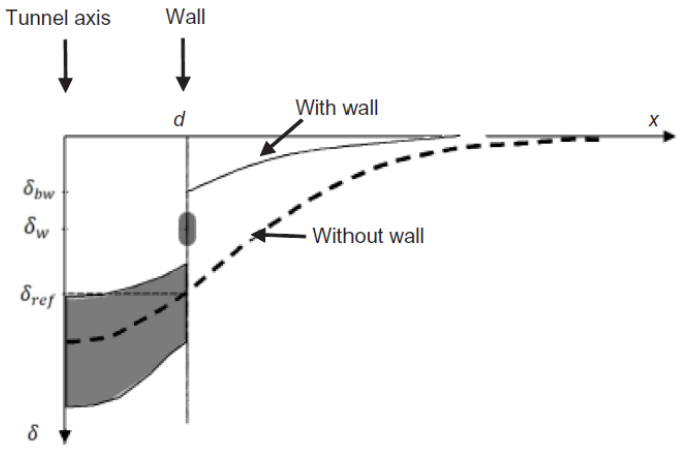

Figure 17- Description of settlement behind a wall, δ_{bw}(adapted from Bilotta, 2008).

For a better understanding of the embedded diaphragm behaviour, Figures 18 to 21 plot the efficiencies of rough walls at the same volume loss (1.35%), at two different offsets from the tunnel axis (1Dt and 1.5Dt). In the charts, the continuous lines plot the computed numerical results while dashed lines represent the centrifuge results

The results displayed in Figure 18 show that rough walls attained negative local efficiencies values irrespective the wall height for almost all centrifuge tests and almost all numerical analyses, except when the embedded wall had a total height of 120mm. Additionally, as displayed in Figure 18, Bilotta, 2008 points out that there is an increasing trend toward positive

values when the wall height increases. However, Bilotta, 2008 alleges that from these results, it can not be stated that by increasing the wall height, the local efficiency rises indefinitely.

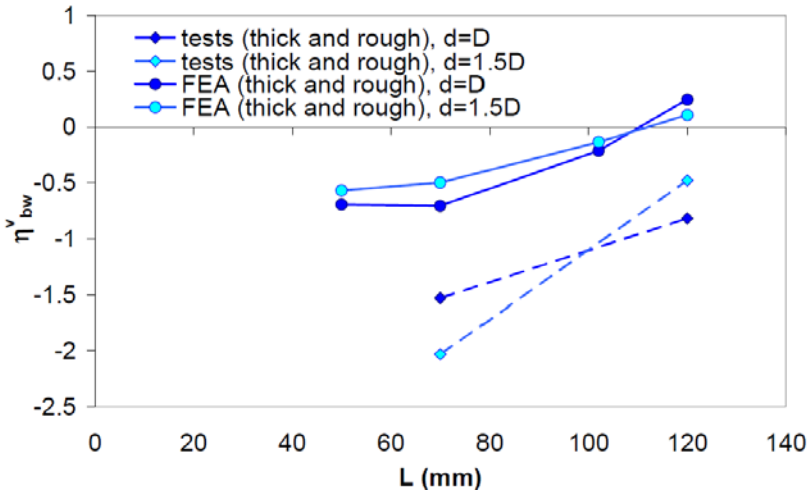

Figure 18- Local efficiencies computed from numerical analyses and centrifuge tests (Bilotta, 2008).

Bilotta, 2008 also alleges that the negative values from Figure 18, may be linked to the wall weight. In order to support this allegation, a similar analysis was carried out setting the wall unit weight equal to the soil, excluding the impact of the additional weight, as displayed in Figure 19. This figure displays the influence of the unit weight in the local efficiency of the wall, by comparing "heavy" walls to "light" walls (unit weight equal to the surrounding soil). Bilotta, 2008 concludes from the results of Figure 19 that the wall self-weight is an important parameter to take in consideration, because of thick and "light" walls attain better local efficiency values (around 50% of efficiency) than thick and "heavy" walls(around 25% of efficiency).

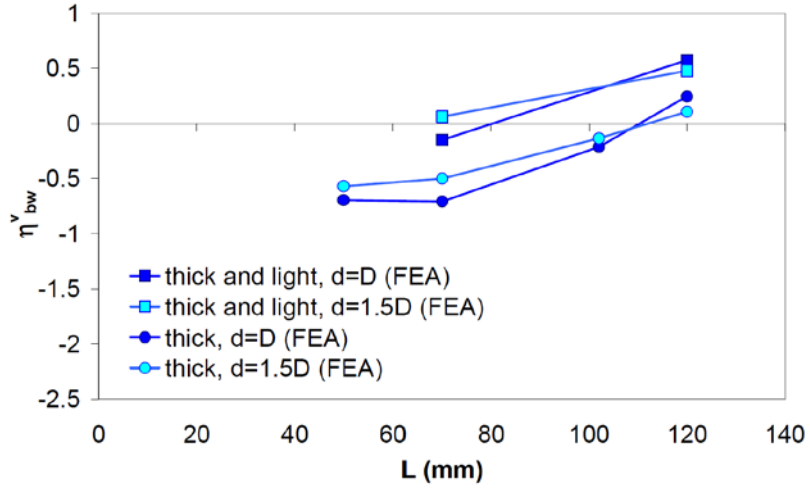

Figure 19-Influence of the wall unit weight in the computed efficiency parameter from numerical analyses (Bilotta, 2008).

In order to study the influence of the embedded wall stiffness on the local efficiency parameter, Bilotta, 2008 performed numerical analyses for different embedded wall stiffness ("thin" and "thick") at the same unit weight as the soil (light). Figure 20 displays the results from this influence on the local efficiency parameter. According to Bilotta, 2008, from the plotted results, it is possible to observe that the computed efficiencies are nearly the same. Thus, Bilotta, 2008 suggests that the embedded wall stiffness is not a relevant parameter that sensibly affects the local efficiency parameter irrespective of its height.

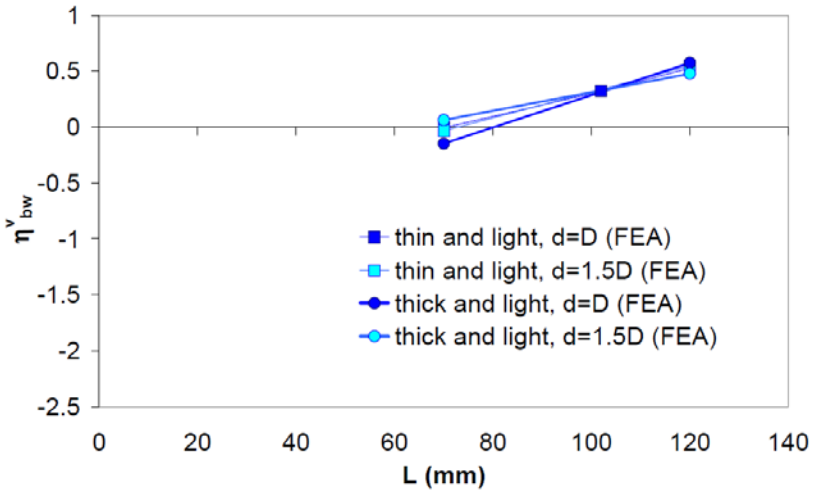

Figure 20- Influence of the embedded wall stiffness in the computed efficiency parameter from numerical analyses (Bilotta, 2008).

Bilotta, 2008 also performed centrifuge tests and numerical analyses to investigate the influence of the roughness interface of the embedded wall on the efficiency parameter. From both analyses, the results displayed in Figure 21, Bilotta (2008) points out that the efficiency parameter of smooth embedded walls was positive in these cases. However, it is worth noting that, overall, the centrifuge tests attained higher efficiency values than the numerical analysis. In the case of increasing the height of the embedded wall (L=1.5C to 2.5C), there is a slight increase in the local efficiency for the centrifuge test. Conversely, the local efficiency had a sharp increase when the embedded wall was extended in the numerical analysis.

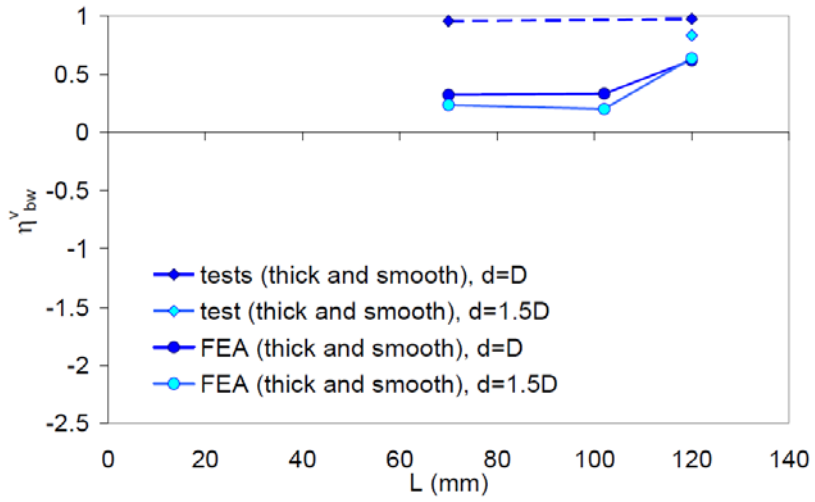

Figure 21- Influence of smooth interfaces of embedded walls in the computed efficiency parameter from numerical analyses (Bilotta, 2008)

3.2.2 Rampello et al. (2019)

Rampello et al. (2019) performed several numerical analyses in order to assess the efficiency of an embedded wall, either continuous or as a line of piles, to prevent damage to existing buildings alongside the tunnel. A two and three-dimensional FE analysis was carried out in order to understand the main mechanisms of the soil-barrier interaction.

The embedded wall was assumed of either finite or infinite in horizontal extension (plane strain condition), to evaluate the length required to obtain in a given section a settlement reduction similar to that attained under plane strain conditions. Furthermore, Rampello et al. (2019) studied the effects induced by the wall installation and the influence of a building nearby in the performance of the embedded wall.

The reference study was based on the section T3 of Line C of Rome Metro network. The tunnel has an outer diameter D_t=6.7m, and is located at 25 m depth from the building foundation (z_0). The ground conditions were similar to those encountered in the historical centre of Rome and consist of 17 m of gravelly made ground (MG), overlying alluvial deposits of the Pleistocene age, 13 m of over-consolidated sandy silt. The mechanical behaviour of the sandy silt was described using the Hardening Soil model with Small Strain Stiffness (HSsmall), while the behaviour of MG was described by the Hardening Soil model (HS). The embedded wall, made of concrete piles of diameter D_p=0.6m were modelled as elastic materials with a Young's

modulus E_{Wall}=31GPa and a Poisson ratio ν=0.15. The contact between the piles and the soil was assumed either fully or partially rough (Rampello et al., 2019).

The three-dimensional FE analyses of a discontinuous embedded wall made by a line of piles were limited to an offset of d= 0.8Dt from the tunnel axis. The length (L) of the embedded wall was assumed to be either: z_0+0.5D_t; z_0+D_t or; L=z_0+1.5D_t from the tunnel axis, where z_0 corresponds to the depth of the tunnel axis (Rampello et al., 2019).

Figure 22 displays the three-dimensional finite element model and the mesh adopted for the line of piles with 7.2 m in the longitudinal extension parallel to the tunnel, simulating an endless longitudinal extension. The line of piles with 12, 8, and 6 piles was installed in the model that correspond to the spacings of s=D_p, s=1.5D_p, and s=2D_p, respectively, In total, the model has 50 m by 180m in the transverse cross-section (Rampello et al., 2019).

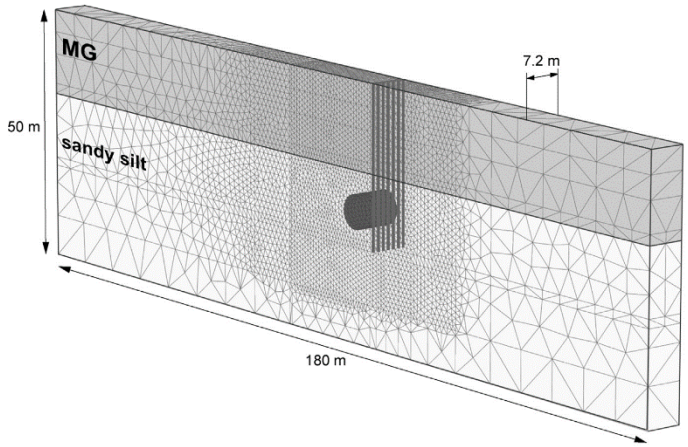

Figure 22- The 3D FE mesh adopted using a line of piles (adapted from Rampello et al., 2019).

To simulate a limit scenario for which the mitigation technique might be needed the value of volume loss was set to 1%. Rampello et al. (2019) defined the effectiveness of the embedded line of piles by comparing the settlements in the presence of the wall and in greenfield conditions. A local efficiency, similar to that defined by Bilotta (2008), was established for a given distance x from the embedded wall (equation 3.2):

$$\eta_{loc}(x) = 1 - \frac{\delta_{bw}(x)}{\delta_{ref}(x)} \tag{3.2}$$

In that $\delta_{bw}(x)$ is the settlement computed in the presence of a barrier and $\delta_{ref}(x)$ represents the settlements computed in greenfield conditions.

Additionally, Rampello et al. (2019) suggested another additional dimensionless ratio to assess the wall's efficiency. The integral efficiency, η_{int}, uses the volume per unit length of the transverse settlement trough computed behind the wall and compares them with and without the embedded wall(equation 3.3). This approach provides an overall index of the volume reduction of the settlement trough behind the wall.

$$\eta_{int} = 1 - \frac{\int_{xb}^{xm} \delta_{bw}(x)\mathrm{dx}}{\int_{xb}^{xm} \delta_{ref}(x)\mathrm{dx}} \tag{3.3}$$

In that, x_b and x_m are the abscissa from the external side of the barrier and the distance for which $\delta_{bw}(x) = \delta_{ref}(x)$ (Rampello et al., 2019).

The integral efficiency results of a line of piles with infinite horizontal extension were assessed through 3D analyses. Assuming a rough interface (R_{int}=1), Figure 23 displays the integral efficiency versus the embedded wall height, where the continuous line represents the diaphragm wall, and the dashed lines correspond to the line of piles installed with different spacing. The results depicted in the figure reveal that the values of the integral efficiency decrease considerably with the increase of the pile spacing. Conversely, the integral efficiency rises with the increase of the embedded wall height. It is also possible to detect a similar integral efficiency for piles spaced at one diameter and for the continuous wall, where a maximum of integral efficiency of about 60% is achieved for L= 35 m (Rampello et al., 2019). The results from the same figure also reveal that the embedded wall attained the highest integral efficiency (around 39%) for the shortest wall (z_0+0.5D_t)when comparing to the line of piles.

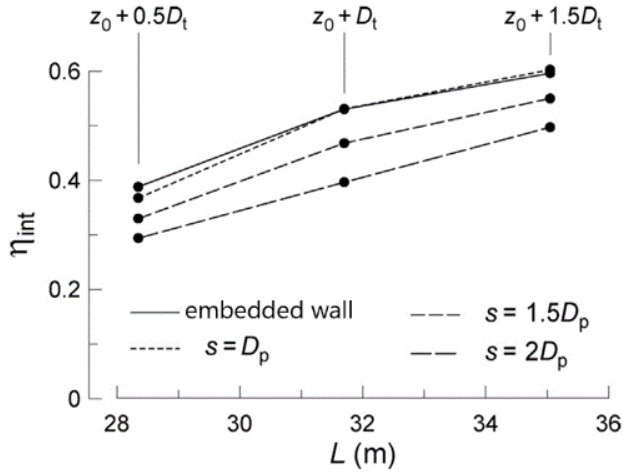

Figure 23- Integral efficiency of a 3D analyses for a continuous line of piles and a diaphragm wall versus barrier height ($R_{int} = 1$) (adapted from Rampello et al., 2019).

Rampello et al. (2019) also assessed the influence of the interface roughness on the integral efficiency parameter of the line of piles. Table 3.1 provides a comparison between the values of integral efficiencies by assuming a "rough" (R_{int}=1) and "smooth" interface (R_{int}=0.7). The results from this table reveal a slight difference between integral efficiencies (≤2% when s=D_p), which suggests are a negligible influence of the roughness interface for small spacing.

Table 3.1- The roughness interface influence on integral efficiency (z_{ref}=4.5m) (Rampello et al., 2019).

	η_{int}					
	$R_{int}=1$			$R_{int}=0.7$		
	$s=D_p$	$s=1.5\,D_p$	$s=2\,D_p$	$s=D_p$	$s=1.5\,D_p$	$s=2\,D_p$
$L=z_0+0.5D_t$	0.37	0.33	0.29	–	0.31	0.23
$L=z_0+D_t$	0.53	0.47	0.40	0.52	0.40	0.29
$L=z_0+1.5D_t$	0.60	0.55	0.50	0.58	0.49	0.41

In respect to the embedded wall stiffness influence on the efficiency parameters, Rampello et al. (2019) performed numerical analyses by reducing the E_{Wall} to 60%, 40%, and 30% of the reference value, as well its unit weight (94%; 88%; 82%). For the cases where the embedded wall height was L=z_0+D_t and L=z_0+1.5D_t, Rampello et al. (2019) suggested a negligible reduction in the computed efficiencies, around 1.5% to 4%.

Regarding the effect of the wall installation, Rampello et al. (2019) did not carry out a study simulating stress changes in the soil caused by the construction of a line of piles. Alternatively, the authors simulated the stress changes of the soil during trenching and concreting of a continuous diaphragm wall. Rampello et al. (2019) alleged that the movements induced by tunnelling prevail over those produced after the wall installation. This allegation was based on the coincident results obtained from the settlement trough in the numerical models when assuming the wall "wished in place" and modelling the embedded wall installation. Accordingly, the authors concluded that the effects of a continuous embedded wall installation could be neglected for designing purposes.

Rampello et al. (2019) also performed a 2-dimensional numerical analysis to study the influence of an embedded wall in the presence of a building. This pertinent numerical analysis aims to study the influence of its structural stiffness and its weight on the shape of the settlement trough. To this aim, an equivalent solid with a simple geometry was embedded down to the foundation level z_{ref}=4.5 m into the soil with a normalised offset (d/Dt) around 1.5.

Table 3.2 presents the results of the local efficiencies in the presence and in the absence of the building. After assuming different values for q_b (building pressure), and E_{eq} (equivalent building stiffness), it is possible to observe that the local efficiency of the wall is mainly affected by the building weight. The building weight modifies the initial effective stress state, and mobilise part of the shear strength of the soil before tunnelling (Rampello et al., 2019).

The results reveal that the local efficiency, in greenfield (tunnel and the embedded wall) and in the presence of the building (q_b =100kPa and E_{eq}=1.0Gpa), was reduced from 0.59 (59%) to 0.37 (37%);. Overall, these results suggested that the efficiency of the embedded wall is reduced in all cases investigated (Rampello et al., 2019).

Table 3.2- Local efficiency in the presence or absence of the building (Rampello et al., 2019).

	q_b (kPa)	E_{eq} (GPa)	η_{loc} (-)
Greenfield	0	0	0.59
Building	50	1.0	0.54
	70	0	0.47
	70	0.8	0.51
	70	1.0	0.51
	70	1.2	0.51
	100	1.0	0.37

3.3 Discussion of results and design recommendations

Based on the studies published in the literature for particular cases, and particularly on the reference works aforementioned, it is possible to summarise some design features recommended when using an embedded wall. These considerations are relevant for the design of an embedded wall, in order to attain high-efficiency values and to reduce ground displacements induce by tunnelling. However, it is of interest to note that some design recommendations were unfounded, and the conclusions were poor, and they may differ from this work since the ground conditions are different.

- **Effects of the embedded wall's offset:** From the studies performed by Bilotta (2008) and Rampello et al. (2019), it is not possible to make any reliable conclusions in respect to the optimal embedded wall offset from the tunnel. Bilotta (2008) performed only two different wall offsets from the tunnel, while Rampello et al. (2019) performed the analyses at one fixed location.

- **Effects of the wall height (L)**: Bilotta (2008) and Rampello et al. (2019) suggested an extension of least 1.5Dt below the tunnel invert to attain higher values of local and integral efficiency.

- **Effects of the axial and flexural wall Stiffness:** Bilotta (2008) alleged that this parameter is irrelevant for the local efficiency. Similarly, Rampello et al. (2019) pointed out a negligible decrease in the computed efficiency when the axial and flexural stiffness was reduced. However, this conclusion is based only by the local and integral efficiencies parameters of the embedded wall for given ground conditions.

- **Roughness interface effect:** Bilotta (2008) suggested that continuous embedded walls with a smooth interface attain higher efficiency values when compared with rough ones. In the case of a discontinuous line of piles, Rampello et al. (2019) pointed out that there is a negligible influence on the efficiency parameters in case of a line of piles for small spacing.

- **The effect of pile Spacing:** the results of numerical analyses demonstrated that the pile spacing should not be higher than 1.5Dp in order to avoid a significant reduction of the wall's efficiency. The effectiveness of a line of piles is directly associated with the pile spacing. As the pile spacing decreases, it approximates to a continuous embedded wall (Rampello et al., 2019).

- **Effects of the wall installation:** Bilotta (2008) neglected the effect of the wall installation, but considered the embedded wall weight, by assuming it as "wished in place". In contrast, Rampello et al. (2019) studied the effects of continuous embedded wall construction and concluded that the induced movements induced by tunnelling prevail over those induced by the wall installation.

- **Effects of the building weight and stiffness:** the study performed by Rampello et al. (2019) concluded that the building weight and stiffness modify the settlement trough. Consequently, it reduces the local wall's efficiency.

- **Effect of the unit weight of the embedded wall:** Bilotta (2008) pointed out that as the embedded wall unit weight increases relatively to the unit weight of the neighbouring soil, its local efficiency decreases. In contrast with Bilotta (2008), Rampello et al. (2019) suggested a negligible influence of the wall unit weight on the computed integral efficiency.

After a careful review of the studies presented, it is possible to take in consideration some suggestions and design recommendations from Bilotta (2008) and Rampello et al. (2019) for the embedded wall design. However, these suggestions must be carefully interpreted due to the

distinct approach from the authors in calculating the efficiency parameters of the embedded and the ground conditions of each study.

This work presents a set of three parametrical analyses that were carried out to explore:

- **The influence of the location and depth of the embedded wall**: Given that the authors did not perform any numerical analyses for various locations and depths, this parametrical study seems to be relevant. The optimal location and depth, for the given stratigraphy presented in the problem, can be found. The cost of the embedded wall may be directly affected by this parameter.

- **The influence of the stiffness of the embedded wall**: Given that the authors did not investigate the forces mobilised along the tunnel and the embedded wall, changes in the stiffness of the embedded wall seems to be a relevant parameter to be studied that could influence the forces mobilised in the tunnel lining. The cost of the embedded wall may also be directly affected by this parameter.

- **The influence of the stress relief factor**: Since the authors assessed the efficiency of the embedded wall for a constant volume loss, this parametrical study aims to perceive how much a volume loss variation influences the efficiency parameters of the embedded wall.

The forces mobilised along the tunnel and the embedded wall were described and discussed for all the parametrical analyses. This seems to be the key to a better understanding of the soil-embedded wall and tunnel-embedded wall interaction.

In addition, this work presents a new efficiency parameter of the embedded wall that was termed as global efficiency η_{global}. This provides an overall index of the V_a reduction in the presence of the embedded wall, which will be explained in details later.

4 THE CASE OF THE SECTION 63 OF LISBON METRO NETWORK

4.1 Description of Works

The growth of Lisbon city at the end of the 19th century resulted in a lack of available and affordable land that induced a new idea of designing an alternative mean of transportation, an underground construction network. However, before the 2nd World War, the Portuguese government did not support this idea. After the end of the war, the financial support of the Marshall Plan allowed the launch of the first line of the Lisbon Metro, the Blue line. Since then, the Lisbon metro network expanded exponentially, connecting different places of the city with the new constructions of the Green, Yellow and Red Line (Figure 24) (Pedro, 2013). The importance of expanding these Metro lines relies on the number of passengers transported every year. The Lisbon Metro estimates that in 2018 the number of passengers reached nearly 169 million, with a growth of 4.7% compared to the previous year (2017). This growth demonstrates the increasing demand of passengers using this mean transportation in the coming years.

The construction methods employed during the excavation of the tunnels of the Lisbon Metro had an evolution over time. The majority of the first sections constructed, up until 1993, were built using NATM, cut-and-cover techniques and mining methods. Since then, and following the trend of tunnelling employed all over the world, the Lisbon Metro acquired the first EPB-TBM machine (see Figure 6). Its first use was on the Green Line excavation, followed by the excavation of the expansion of the Blue Line and of the Red Line. Since then, the majority of the tunnels built for the Lisbon Metro have employed this tunnelling method (Pedro, 2013).

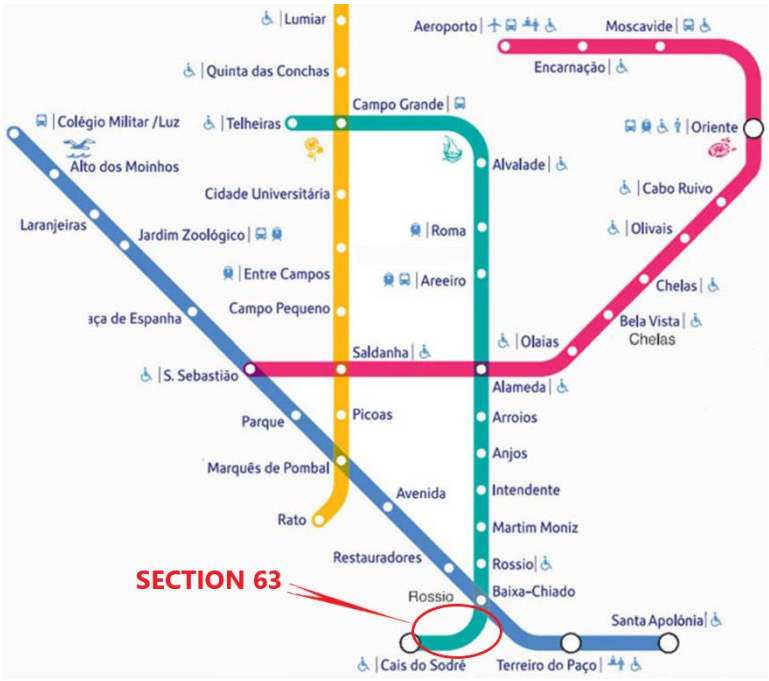

Figure 24- Lisbon Metro network in 2019 (Lisbon Metro, 2019).

This work aims to present and study the case of Section 63 of the Lisbon metro network (Green Line), where the monitoring results presented high values of ground settlements during the tunnel excavation. This section is located between "Cais do Sodré" and the "Baixa-Chiado" stations (Green Line) (Figure 24), which is one of the most important stations since it links the Blue and Green lines, and started its construction using an EPB-TBM in the second semester of 1994 (Pedro, 2013). It is of interest to note that this section stands bellow World Heritage buildings and very degraded structures in a massively dense area of Lisbon (Figure 26b)) (Amaral, 2006). Therefore, Amaral (2006) pointed out that a rigorous instrumentation and monitoring plan to ensure the integrity of adjacent buildings and the stability in the segments of the coating was required, with careful control of the face pressure in the EPB-TBM.

This chapter presents the geometry, geological conditions (stratigraphy), and instrumentation survey and monitoring results between 0+200m and 0+500m of Section 63 (Figure 25). The longitudinal cross-section profile of Section 63 with the different soil layers superimposed is illustrated in Figure 25. The excavation process started from the "Cais do Sodré" station towards the "Baixa-Chiado" station and along the alignment nine cross-sections were instrumented, P4, P5, P6, P7, P8 P9, P10A, P12, and P13, at the locations marked in Figure 26.

The tunnel has a circular section with an external diameter of 9.71m. The lining of the tunnel has 1.2 m long pre-cast concrete segments with 0.36 m thick (Amaral, 2006). Between 0+200 m and 0+500 m of Section 63, the tunnel cover ranges from 9.5 m (P4) to 13.5 m (P14). The alignment is curved, with a maximum radius of 170m, and has a maximum slope of 4%.

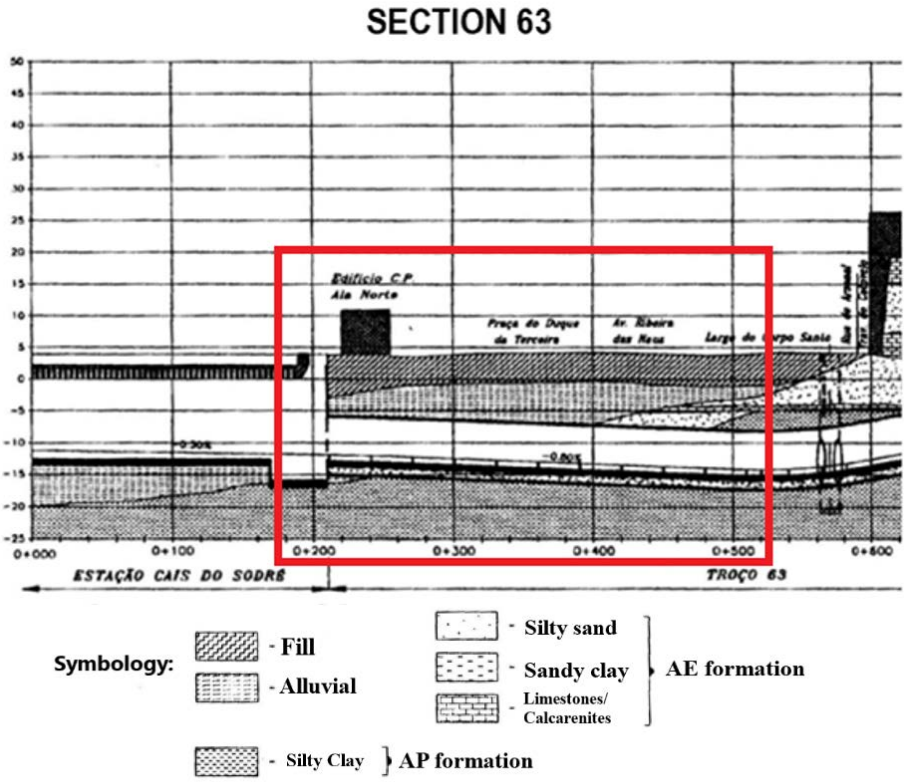

Figure 25- Geological profile and tunnel cross-section of Section 63 between 0+200m and 0+500m (adapted from Amaral, 2006).

Figure 26- Top view from the instrumentation survey from sections P4 to P13 of section 63 in 0+200m to 0+500m between Cais do Sodre station – Baixa/Chiado station.

4.2 Geological-Geotechnical Conditions

At the beginning of the Miocene age, the Atlantic Ocean flooded the Lower Tagus Basin triggering a sedimentation process in a marine-continental interface(Moitinho de Almeida, 2008). In Lisbon, the Miocene deposits have around 300 m thickness, and the alternations between layers suggest multiple shifts of the sedimentation environment (Pedro, 2013). The excavation of Section 63 crosses these Miocene formations, namely the "Argila dos Prazeres" (AP) and the "Areolas da Estefania" (AE) with some limestones intercalations, which overlays recent layers of fill and alluvial soil (Figure 25) and Figure 26). The AP formation has a dark greyish colour suggesting that the sediments were deposited in a marine environment. Laying above the AP formation, the AE formation has a yellowish colour suggesting that the sedimentation process, with different degrees of cementation, occurred in a more oxygenated environment (Pedro, 2013).

The cross-section showing the stratigraphy of the ground profile at the instrumented section P9 (0+300m to 0+350m) is illustrated in Figure 27a). This figure displays that the tunnel is excavated underneath the alluvial/fill soil layer while crossing the AE formation, with a tunnel cover C of 15 m. In Figure 27 b), it is displayed stratigraphy of the ground profile from section P10A (0+300m to 0+350m) with nearly the same cross-section as section P9. The water table is located at 2 m depth. As can be seen in the figures, the different soil formations that occurred at the face of the excavation suggest the complexity of controlling the face pressure by the EPB-TBM. It is of interest to note that the asymmetric stratification is a relevant characteristic from these sections because it influences the shape of the settlement trough. The ground conditions of the right side of the tunnel, where the Tagus river is located, indicates poorer ground conditions, in terms of strength and deformability compared to the left side.

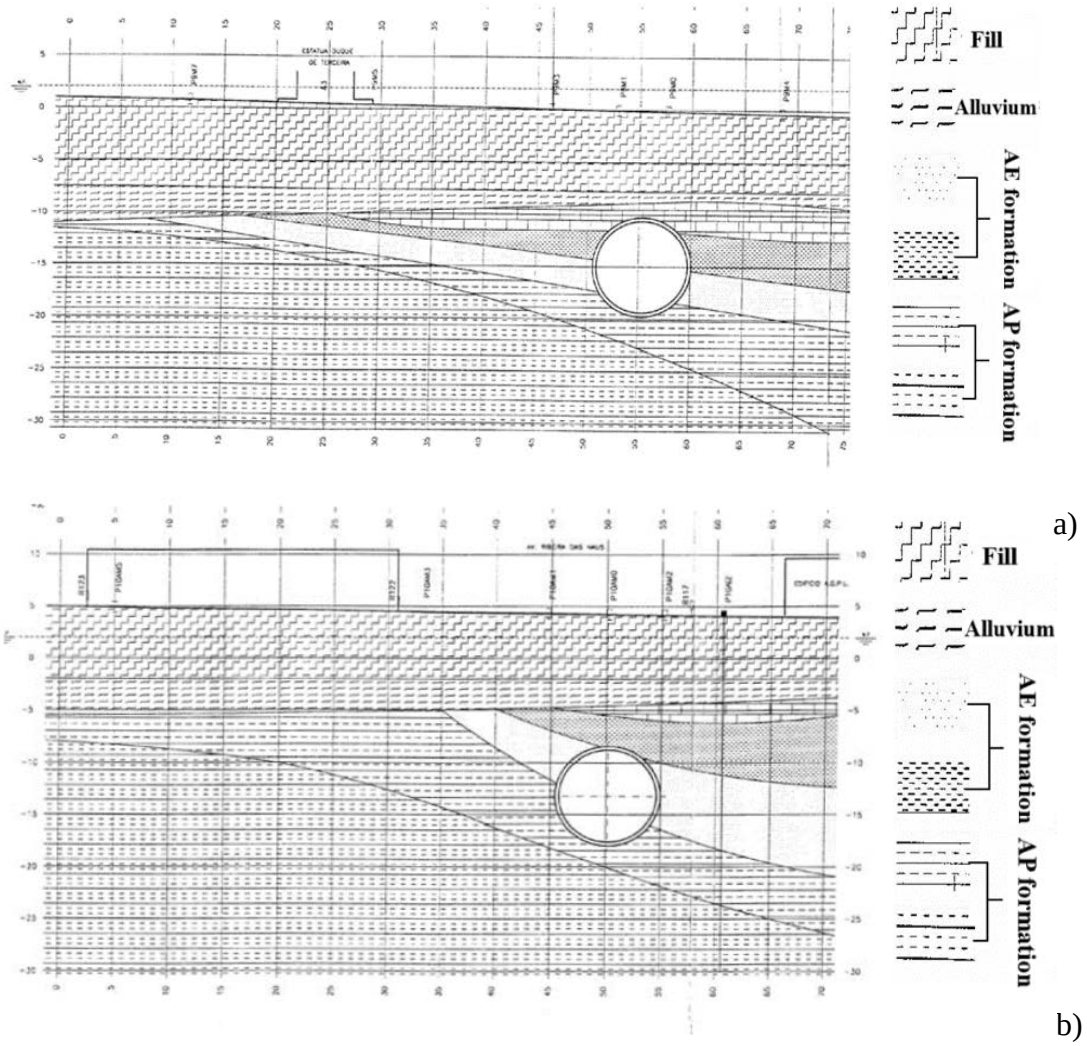

Figure 27- Cross-section of the geology of the instrumented sections: a) P9; b) P10A (adapted from Amaral, 2006).

4.3 Instrumentation Results

The instrumentation survey had as a major objective to measure the surface ground movements in the tunnel vicinity. The frequency of readings was chosen, taking into account the ground behaviour, the type of instrument and the tunnelling speed. Figure 28 displays the typical cross-section of the instrumentation survey installed on the different sections of the Green Line of the Lisbon metro network. Amaral (2006) stated that the instrumented sections had settlement sensors, extensometers, inclinometers, and piezometers eventually installed. However,

settlement sensors the distribution were not always symmetric with respect to the tunnel axis(Amaral, 2006).

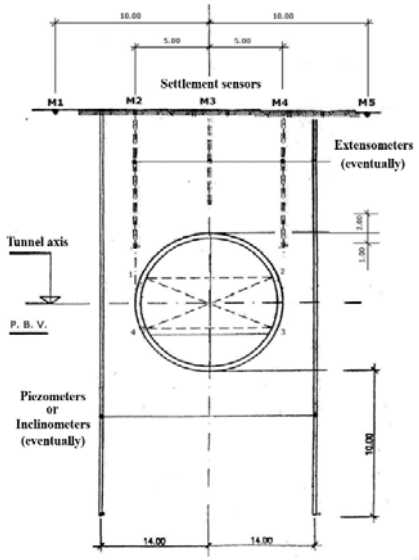

Figure 28- Instrumentation model for cross-section of Section 63 (adapted from Amaral, 2006).

Table 4.1 presents a summary of the maximum final short-term settlements measured ($\delta_{vmax\ measured}$) by settlement sensors. Information about the type of soil layer crossed by the EPB-TBM in each section, the tunnel depth and the best fitting parameters to a Gaussian curve are also displayed. The compiled results of all sections are depicted in Figure 29. The continuous lines on the figure correspond to the Gauss approximation to each cross-section, apart from sections P5 and P7, where there was not enough data to produce a plot. The settlement measured, and displayed in Figure 29 suggests asymmetric settlement trough due to the asymmetric stratigraphy of the ground. This is a relevant note because it implies that this settlement trough could not be approximated fairly by Gaussian curves.

Amaral (2006) alleged that the instrumented sections P4, P5, and P6 were excavated under jet-grouting columns protection. For the particular case of the instrumented section P4, it was registered a small maximum settlement value measured in the field ($\delta_{vmax\ measured}$ =6.5 mm) . However, from the $\delta_{vmax\ measured}$ of the instrumented sections P5 and P6, Amaral (2006) alleged a low efficacy of this protection, which was around 36.4 mm and 35.9 mm, respectively. Thus, in the following instrumented sections (from P7 to P14), Amaral (2006) pointed out that compensation grouting treatment was performed in each of them.

In order to control and reduce the measured settlements in the subsequent section (P7), the EPB-TBM face pressure was increased. However, this face pressure increase was disproportionate, causing some minor heave before the passage of the shield. Hence, it was registered a

$\delta_{vmax\ measured}$= 42 mm . After section P7, the EPB-TBM face pressure was reduced and controlled, minimizing the heave before the passing of the shield. The subsequent section P8 attained $\delta_{vmax\ measured}$= 37.9 mm, lower than the previous section.

From Table 4.1 and Figure 29, it is possible to verify the highest value of the $\delta_{vmax\ measured}$, around 66.9 mm, from section P9 when compared to those of other sections. Additionally, this section presents a small value for the trough width factor (i=4.6 m), implying the narrowest and concentrated settlement trough, as observed in Figure 29. Naturally, these results correspond to substantial values of the angular distortion and horizontal tensile strain. Amaral (2006) suggested that this behaviour could be linked to the low efficiency of the compensation grouting treatment, as well for sections P9 and P10A.

After section P9, the $\delta_{vmax\ measured}$ was sensibly reduced to 36.4 mm in section P10A, though still high. After that, sections P12 and P13 attained low $\delta_{vmax\ measured}$, 17.2 mm and 12.1 mm, respectively.

Table 4.1- Parameters from the settlement trough cross-sections of Section 63 (Amaral, 2006).

Section	Crossing Layer	Tunnel Depth	δmax measured (mm)	i (m)
P4	Alluvial Soil	14.6	6.5	14.6
P5		14.5	36.4	-
P6	Alluvial Soil / AP formation	15	35.9	10
P7		15	42	-
P8	AP formation	17.1	37.9	8.4
P9	AE formation	15	66.9	4.6
P10A		17.5	36.4	6.3
P12		16.2	17.2	15.1
P13		17.5	12.1	12.2

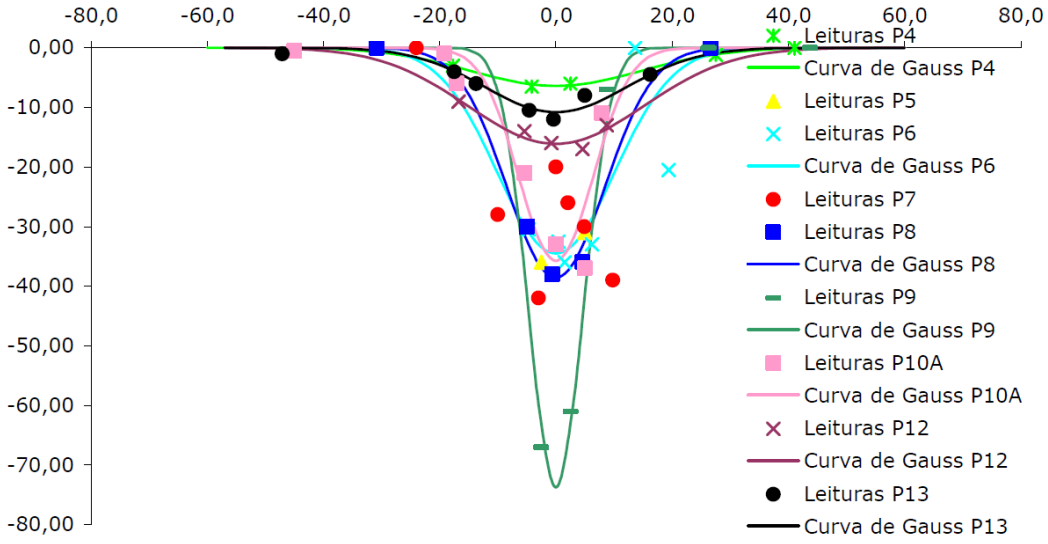

Figure 29- Settlements measured and Gauss approximation at the instrumented (Amaral, 2006).

5 ASSESSMENT OF THE EFFICIENCY OF AN EMBEDDED WALL

5.1 General Considerations

This chapter aims to present the influence of using an embedded wall as a preventive measure to mitigate the settlements that might affect the buildings located at Section 63. In particular, sections P9 and P10A (see Figure 26) were selected since, despite having a similar ground profile, they presented significant discrepancies in terms of settlements. Naturally, section P9 was adopted for reference in this study as it presented the highest settlements measured by the instrumentation ($\delta_{vmax} = 67\ mm$) in comparison with the observed in the other sections.

The numerical analysis was conducted assuming plane-strain conditions and performed using RS2 v2019 software. The performance of the embedded wall was assessed by the settlement and V_a modifications using the aforementioned indexes or similar. Additionally, the forces mobilized on the tunnel and also on the embedded wall are also presented and discussed.

5.2 Numerical Models

5.2.1 Geometry, mesh and boundary conditions of the FE models

Two models were considered for the analysis:

- Greenfield model, i.e. without the existence of any structure besides the tunnel;
- Reference modelling, when prior to the tunnel excavation, an embedded wall is installed at a pre-defined distance from the tunnel axis.

The geometry of both models is identical, apart from the elements that simulate the embedded wall. The adopted ground stratigraphy had as reference the profiles of section P9 (Figure 27a)) and P10A (Figure 27b)), which were merged into a unique model that despite some simplifications can still be considered representative of the ground profile on both sections.

Figure 30 illustrates the two-dimensional model employed, which has 150m width and a height of 33.2 m. The tunnel with a diameter Dt= 9.71m is centred in the model and as a cover

C=11.4m (C/Dt=1.17). This value is an average of the cover measured in sections P9 (10.15m) and P10A (12.65m).

As mentioned previously, the same model but now with an embedded wall adjacent to the tunnel was installed and considered for the reference analysis. The embedded wall was located on the side of the Tagus river, right of the model, since it is where the soil conditions are more unfavourable. An offset from the tunnel axis of d=12.1m (d/Dt=1.25) was considered for the embedded wall, which had a total height of 23.53m (extended below the tunnel centre h=0.75Dt).

The model discretization was carried out by subdividing the domain into 6-noded triangles finite continuum elements. The embedded wall and the lining of the tunnel were simulated using beam elements. The mesh was refined enough to have a good performance around the tunnel and the embedded wall. The domain has a total of 6319 elements and 13009 nodal points in the greenfield model; while the reference modelling has 6404 elements and 13234 nodal points.

Figure 30 shows the mesh adopted for the greenfield numerical model, while Figure 31 shows the mesh details for the reference modelling with the embedded wall with h=7.28m (h/Dt=0.75), and d=7.28m (d/Dt=0.75). The sequence of the different layers of the soil considered is visible on the figures.

In respect to the boundary conditions, a “free surface” was considered on top, rollers on the lateral sides (restrained in the horizontal direction) and pinned on the bottom (restrained both in the vertical and horizontal axis). The hydraulic properties from the ground were also taken into account in the model. In agreement with the site measurements, the water table was considered located at 1.2m depth. In order to simulate a constant and permanent flow to the model, a 32m piezometric level in the lateral sides of the model was imposed. Besides that, as a hydraulic condition, in the perimeter of the tunnel, a boundary of no pressure (P=0) was prescribed. This intended to simulate the drainage of the ground that occurred during the excavation. Even though this is not a realistic hypothesis, particularly considering the long term and the tunnel impermeabilization, the objective of this work was to replicate the short-term behaviour and consequently it was considered this boundary as the most adequate for this purpose. The embedded wall was considered to be impermeable. It should be noted that suctions generated by the hydraulic equilibrium were considered equal to zero in all analyses.

In order to replicate as accurately as possible the excavation process, it was decided to consider the solid-fluid interaction as partially coupled analysis. In this option, the RS2 v2019 program considers that changes in the pore pressure and in the effective stress affect deformation. However, variations in loading or deformation do not affect pore pressure. As a result, for each

stage, the program begins by calculating the hydraulic equilibrium based solely on the hydraulic boundary conditions prescribed and on the permeability of the formations. After the program includes the determined pore pressures in the effective stress analysis and determines the associated deformations, that, in turn, do not affect the pore pressure distribution initially determined.

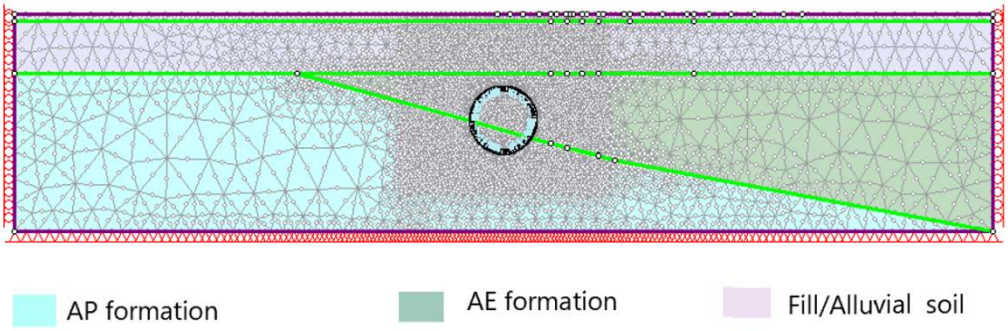

Figure 30- The mesh discretization of the numerical model in greenfield conditions.

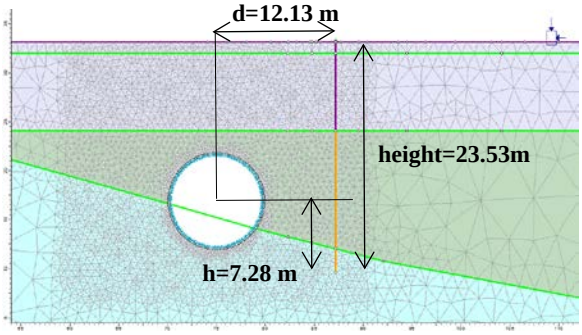

Figure 31-The mesh from the reference modelling with the presence of the embedded wall.

5.2.2 Materials models

In order to simulate the ground behaviour, the elastic-perfectly plastic model with the Mohr-Coulomb failure criterion was chosen. The reason for choosing this model is based on its simplicity, which requires fewer parameters with physical meaning widely known in the engineering field.

In the elastic range, the model's stress-strain behaves linearly, based on two-state parameters from the Hook's law, the Young modulus, E, and the Poisson's ratio, ν. In the elastic range, the Young modulus E remains constant; however, in the perfectly plastic phase, the strains increase with no restriction while the stress remains constant.

In order to define the failure criteria and plastic behaviour, there are three parameters required: cohesion, c', shearing friction angle, ϕ', and dilatancy angle, ψ'. In order to characterise the

flow rule, associated or non-associated, the dilatancy angle is defined to simulate the irreversible change in volume during shearing. In the case of the potential plastic function is the same as the yield function, the flow rule is called associated ($\phi' = \psi'$). In the case of the potential plastic function be different from the yield function, the flow rule is called non-associated ($\phi' \neq \psi'$). In this work, the dilatancy angle was set to zero, meaning that zero plastic dilatation occurs (i.e. non-associated flow rule) (Potts et al., 2001).

The benefit of using the non-associated flow rule is a restriction of the generation of incremental plastic volumetric strain. However, the model still predicts an increase in the volumetric strains irrespective of how far the soil is sheared, which is an unrealistic behaviour (Potts et al., 2001).

It is of interest to note that according to Addenbrooke et al. (1997); Hejazi et al. (2008), the use of an elastic-perfectly plastic model with Mohr-Coulomb failure criterion leads to a shallower and wider shape of the settlement trough than the results observed in experiments. In order to get around with this problem, the solution is to take into account some of the fundamental aspects of soil behaviour. These include the variations of the dilatancy angle before shearing, the variation of modulus in respect to the stress state, and modulus in loading different from that in unloading. Thus, this requires to use at least an elastoplastic constitutive model with isotropic hardening (Hejazi et al., 2008). However, the use of an elastoplastic constitutive model with isotropic hardening was not employed in this study, since it requires a high number of parameters during the calibration process.

The parameters adopted in this model were obtained from the literature: Pedro (2013), Matos Fernandes (2006), and Ferreira (2014) based on empirical correlations and experimental tests. Table 5.1 presents the strength, stiffness, and permeability parameters required to model the different geotechnical materials using the constitutive elastic-perfectly plastic Mohr-Coulomb model. Due to the low permeability of the Fill/alluvial soil and the AP formation, they were considered as undrained material behaviour, which means that they can generate excess pore pressure. Conversely, the AE formation due to its sandy nature was considered as a drained material behaviour (excess pore pressures can not be generated).

Table 5.1 Soil parameters considered in the numerical model.

					Drained/Undrained			
Soil layer	**γ(kN/m3)**	**c'(kN/m2)**	**ϕ'(°)**	**ψ(°)**	**E_{ref}(kN/m2)**	**ν**	**Ko**	**k(m/s)**
Fill/Alluvial Soil	18	0	33	0	10000	0.3	0.5	1.00E-09
AE formation	20	4	42		38500		0.7	1.00E-05
AP formation	20	50	35		43500			1.00E-09

The embedded wall and the tunnel lining were assumed to be made of concrete and were modelled using a linear elastic law. The roughness interface of the embedded wall was simulated as a joint with a peak friction angle of $0.6\phi'$. The lining thickness is 0.36m (Amaral, 2006), while for the reference modelling, the embedded wall has a 0.4m thickness. Table 5.2 summarises the geometrical and mechanical properties of the lining and the embedded wall.

Table 5.2- Summary of the geometrical and mechanical properties of the tunnel lining and the reference embedded wall for the reference modelling.

Geometrical characteristics of the embedded wall and lining				**Elastic Parameters of the embedded wall and the tunnel lining**		
Depth(m)	**Offset (m)**	**t-wall (m)**	**t-tunnel (m)**	**E(GPa)**	**γ(kN/m3)**	**ν**
18.7	12.1	0.4	0.36	30	24	0.2

5.2.3 Construction sequence

The construction sequence adopted consisted of three stages for the greenfield analyses and four stages for the analyses with the embedded wall. Table 5.3 displays a summary of the stages adopted for each case. As mentioned previously, before computing the effective stress-deformation analyses, the hydraulic equilibrium and associated pore water pressures were computed based on the soil permeability and boundary conditions defined for each stage.

The tunnel excavation was divided into two stages by using the stress-reduction method. During the first stage, the initial stresses released due to the tunnel excavation were partially reduced by a stress relief factor α.In the second stage, the lining is installed, and the remaining loads applied. The stress relief factor α was obtained by calibration, as described in the following section.

Table 5.3-Summary description of each stage adopted in the numerical model.

a) Greenfield model	**b) Reference modelling**	
Stage	**Stage**	**Description**
1	1	Initial stress state
-	2	Embedded wall installation
2	3	Tunnel excavation with relief factor
3	4	Installation of the tunnel lining

5.3 Calibration of the Numerical Model

5.3.1 Back-Analysis and Reference Results

The excavation of a real tunnel is a 3-dimensional problem and, therefore, a 2-dimensional analysis in the transversal plane does not account for strains and shear stresses in the longitudinal direction of the tunnel axis. Thus, in an effort to simulate the tunnel excavation in-plane strain conditions, a back-analysis was performed by varying the stress relief factor, α. Its value was calibrated so that the maximum vertical displacements were in agreement with the measured values at the instrumented sections, P9 and P10A.

During the back-analysis, several assumptions for the stress relief factor α was adopted in order to correlate it with vertical displacements. Thus, α was varied between 0.2 and 0.8, with the latter value representing a late installation of the lining. For values of α>0.8, the computed results did not converge. Figure 32 displays the evolution of the maximum displacement on the ground surface in the numerical model with the stress relief factor α. It is of interest to note that for $\alpha > 0.7$, there is a sharp increase in the computed settlements on the ground surface. The given results also can be related to the plastic yield zone developed around the tunnel, where the number of yielded elements increases exponentially for higher values of α.

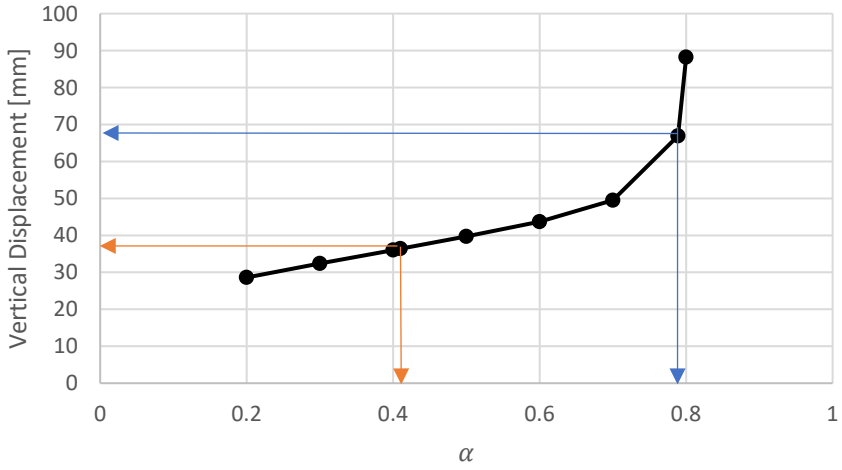

Figure 32 - Relation between vertical displacements and relief factor α

From the instrumentation results, the maximum settlements measured for sections P9 and P10A in the settlement trough were 67 mm and 36.4 mm, respectively. The values the correspondent α were indicated in Figure 32. Table 5.4 summarizes these results for each section.

Table 5.4- Comparison between the settlements (from sections P9 and P10A) obtained from the instrumentation data and numerical results.

Section	Instrumentation (mm)	Numerical (mm)	α
P9	67	66.9	0.789
P10A	36.9	36.4	0.41

Figure 33illustrates the comparison between the instrumentation results and the settlement troughs obtained from the numerical analyses. The results of the maximum settlements obtained in the numerical analyses are in agreement with those measured in the field. However, after comparing the settlement trough shape, it was noted that the settlement trough determined in the numerical analysis was wider than the that measured in the field. The numerical results also reveal higher settlement values on the right side of the tunnel, due to poor soil conditions, which were not observed in the field.

After a proper calibration of the numerical model, the volume of the settlement trough Va, was calculated as a percentage of the theoretical tunnel volume Section P9 and P10A attained Va =3.61%,and 2.70%, respectively in greenfield (see equation 2.4).

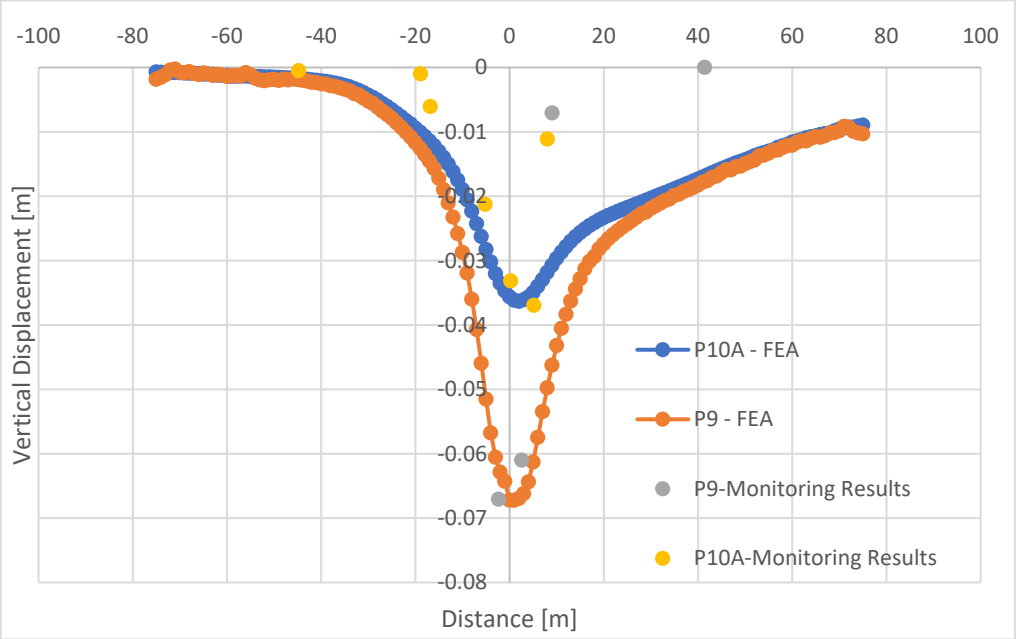

Figure 33- Comparison between the settlement trough obtained from the FEA with and without the reference embedded wall, and the monitoring results from each section (P9; P10A).

The impact of using an embedded wall in the mobilised forces acting on the lining is a relevant aspect to explore. Prior to that, Figure 34 shows the comparison of the axial forces and of the bending moments acting on the lining (clockwise direction, starting from the tunnel crown) for sections P9 and P10A in greenfield conditions. The differences between the two sections reflect the influence of the stress relief factor adopted in the numerical simulation, with lower forces being observed in section P9, where a higher stress relief factor was adopted. In terms of axial forces, the maximum difference between sections P9 and P10A is around 477.58 kN/m at the invert. Generally, the axial force increases with depth (from θ=0° and θ=180°) due to the gravity effect, with the maximum values of 275kN/m and 745.2 kN/m for sections P9 and P10A, respectively. The magnitude of the bending moment is generally small. However, a significant variation occurs between the springline (θ=90°) and the invert (θ=180°), probably associated with the transition from the AE to the AP formation. The maximum absolute value of the bending moment attained is 28.9kNm/m and 8.11kN/m for sections P10A and P9, respectively.

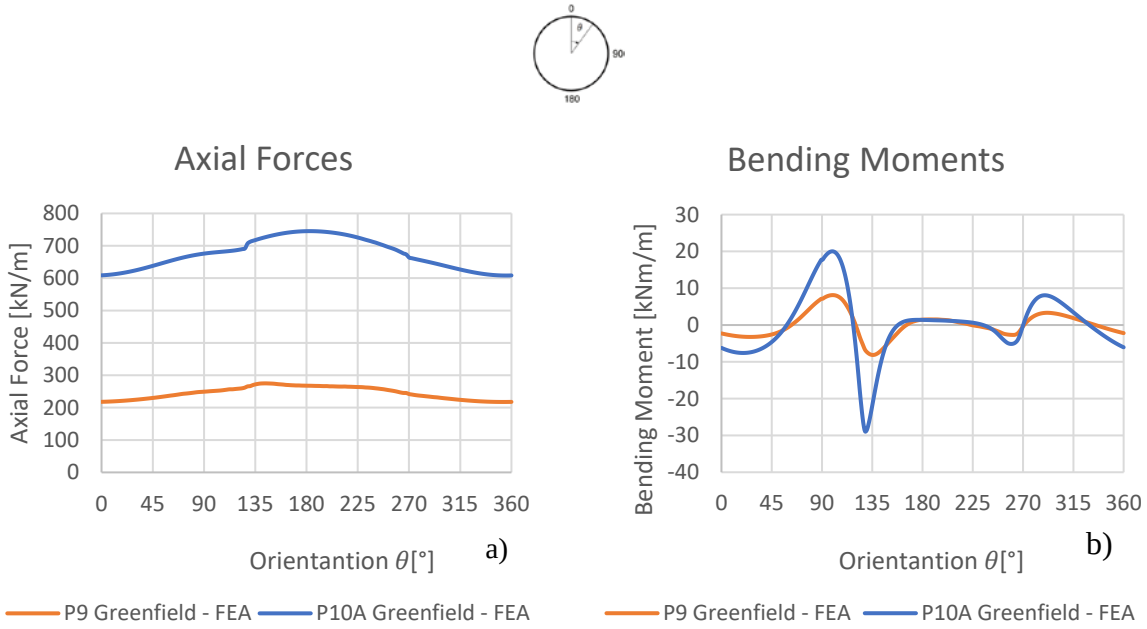

Figure 34-Comparison between axial forces a); bending moments b) from sections P10A and P9, respectively.

5.3.2 Influence of the Embedded Wall Settlements

The influence of the embedded wall (reference modelling) in the settlement trough of section P9 was assessed by using the two dimensionless ratio parameters mentioned in Chapter 3 termed as local efficiency by Bilotta (2008) (see equation 3.1) and global efficiency parameter η_{global}. As aforementioned the first gives a local comparison between the computed settlements with the embedded wall and the settlements in the absence of the wall (immediately behind and in front of the embedded wall), while the latter provides a global indicator of the settlement trough volume variation with the presence of the wall. (equation 5.1). In the equation proposed, V_a is the volume of the settlement trough normalised by the tunnel volume per unit length in greenfield, conditions and V_{aw} is the normalised volume of the settlement trough per unit length after the wall installation.

$$\eta_{global} = \frac{V_a - V_{aw}}{V_a} \times 100 \tag{5.1}$$

When $\eta_{global} = 1$, the embedded wall is entirely effective in reducing V_a. If $\eta_{global} = 0$ the embedded wall is considered entirely ineffective. In the case $\eta_{global} < 0$ the effect of the embedded wall is detrimental (i.e. increases V_a).

Figure 36a), b) and c) illustrate the contours of the vertical displacements obtained in the greenfield and in the reference scenarios for section P9. The embedded wall originates a discontinuity in the displacement field (Figure 36b)), acting as a physical barrier in the ground, which reduces the magnitude of the vertical displacements substantially (Figure 36c)). In order to perceive this reduction, Table 5.5 presents the efficiency of the wall in the reference analysis. The local efficiency computed indicates that the embedded wall has a positive effect in the settlement trough reducing around 32.2% of the settlements in front of the wall, and 79.6% behind the wall. The differences may be associated with the distribution of forces behind/front of the embedded wall since its installation changes the distribution of the settlements around it (Figure 36c)). Additionally, the global efficiency computed shows that the wall reduced the volume of the settlement trough V_a of around 40.7%. A reduction of 11.6% of the maximum settlements, located near the tunnel axis, after the installation of the embedded wall, from 67 mm to 59 mm, was also observed.

Table 5.5- Local and global efficiency computed the reference modelling.

Reference Modelling	Local Efficiency(%)	Global Efficiency(%)
In front of the wall	32.2	40.7
Behind the wall	79.6	

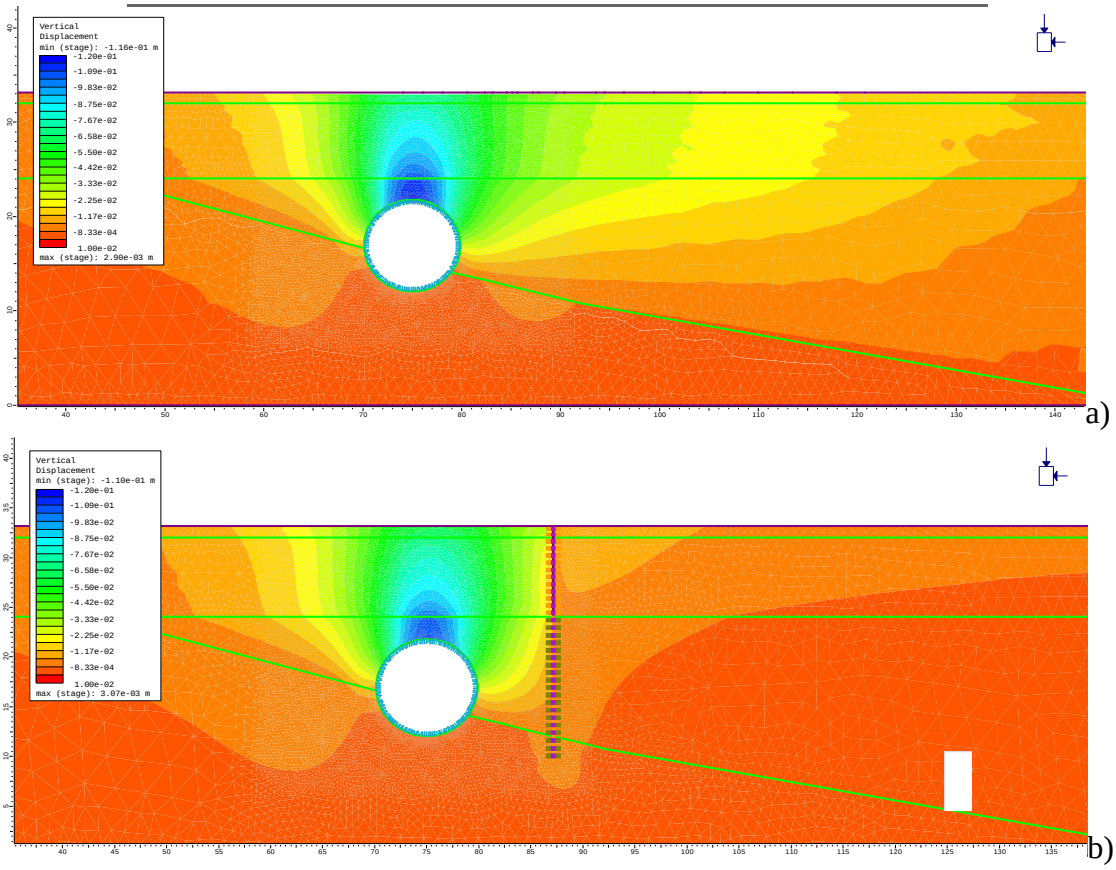

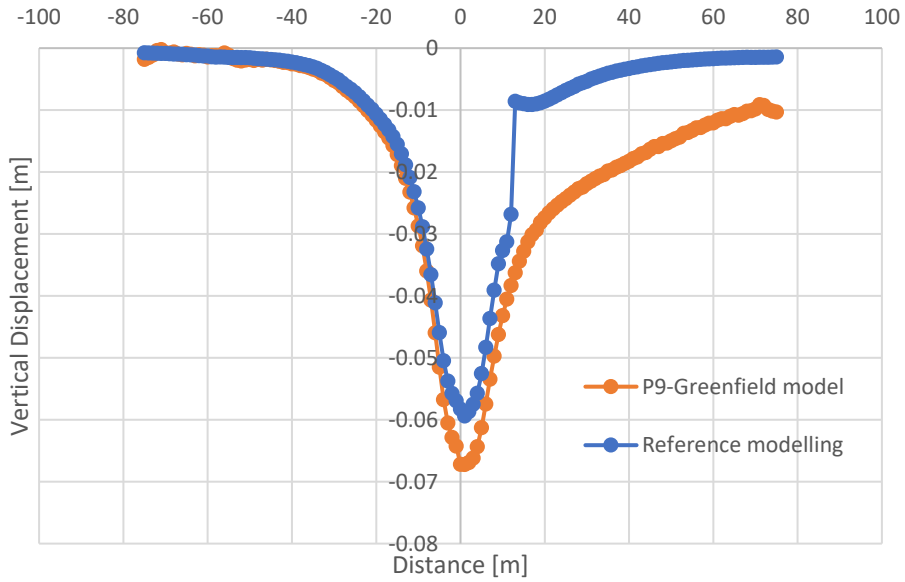

c)

Figure 36- Displacement fields from the numerical models:a) greenfield; b) reference modelling; c) comparison between the greenfield model and reference modelling.

5.3.3 Forces on the Tunnel Lining

The maximum forces mobilised on the tunnel lining before and after the embedded wall installation are presented in Table 5.6. Figure 37a) illustrates the comparison between the axial forces on the tunnel lining in the greenfield model and with the embedded wall (reference modelling), while Figure 37b) illustrates the variations in the bending moments. The development of the axial forces increases with depth from θ=0 and θ=180°, regardless the presence of the embedded wall. However, there is a minimal decrease in the axial force from 275kN/m to 270kN/m at 140°, after the embedded wall installation. Thus, it can be concluded that the embedded wall at this location does not affect the axial forces in the lining substantially. The changes in the magnitude of the bending moments seem to be irrelevant. A negligible decrease from 8.11kN.m/m to 7.58 kN.m/m at 140°, while a negligible increase occurs at 135° from -8.13kN.m/m to -8.11kN.m/m. Thus, it can be concluded that the embedded wall does not affect the distribution of the bending moments substantially along the lining.

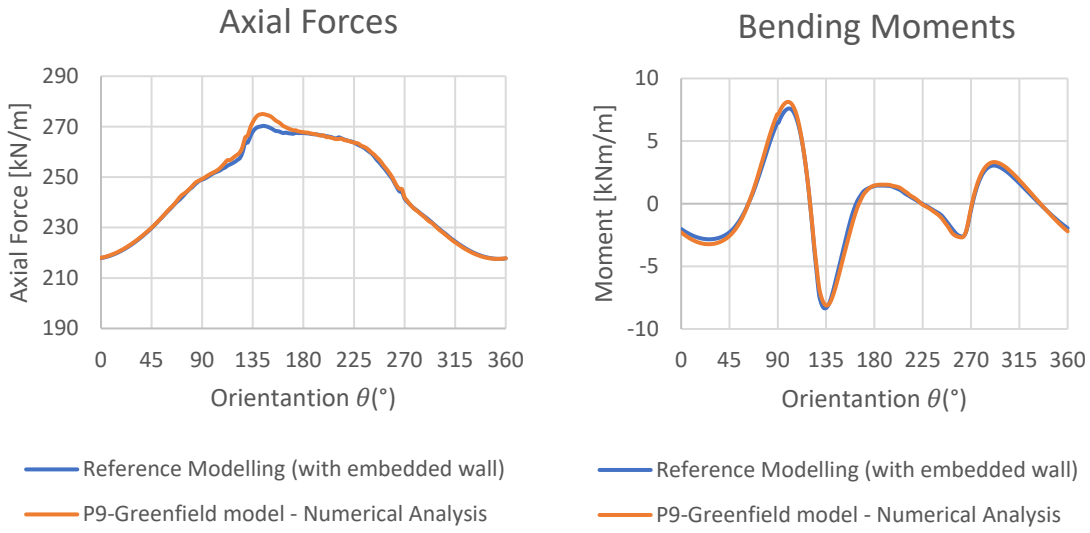

Figure 37-Comparison between the forces acting on the tunnel lining: a) axial forces; b) bending moments.

Table 5.6- Summary of the forces acting on the tunnel lining.

With Wall			Without Wall		
Nmax(kN)	**Mmax(kN.m)**	**Mmin(kN.m)**	**Nmax(kN)**	**Mmax(kN.m)**	**Mmin(kN.m)**
270.302	7.599	-8.352	275.00	8.13	-8.13

5.3.4 Forces on the Embedded Wall

The forces mobilised and the horizontal displacements along the embedded wall are displayed in Figure 38a), b) and c), respectively, for the reference modelling at the last stage. It is interesting to note that the maximum bending moments occur in the transition between the Fill/Alluvial soil and the AE formation, around -93.04kN.m/m., which seems to be very high compared to the values attained at the toe of the wall (21.29kN.m/m). The probable reason for this is a concentration of forces acting in the transition zone. In respect to the axial forces, there is an increasing trend (due to the gravity effect) that reached a maximum of 679.08kN/m at approximately 20m depth, after that the axial forces have a slight decrease to about 583.75kN/m at the toe. One reason for this effect could be related to the upward friction acting on the embedded wall due to the upward ground displacement caused by the excavation. The horizontal displacements observed, around 22.4 mm near the ground surface are justified due to the horizontal movements that occur towards the tunnel excavation.

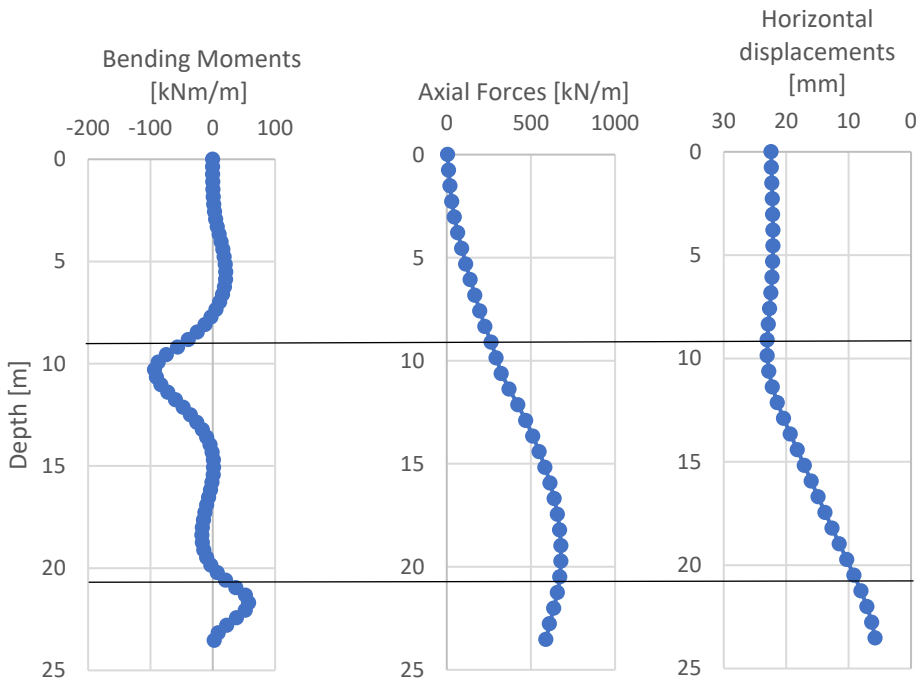

Figure 38- Distribution along in depth the embedded wall: a) bending moments; b) axial forces; c) horizontal displacements.

6 PARAMETRIC ANALYSES

6.1 General Considerations

In order to evaluate the main factors affecting the performance of the embedded wall, several parametric analyses were carried out. In these analyses, the embedded wall location, depth, and stiffness were varied. Additionally, the influence of the stress relief factor, α, in the efficiency of the embedded wall was investigated.

The magnitude of the impact of the embedded walls in the settlement trough was assessed based on their local and global efficiency. Additionally, it was investigated the influence of the embedded wall on the forces acting on the lining of the tunnel and along with the depth of the wall. The comparison was carried out relative to the greenfield model, where the maximum and minimum forces (N_{max} ; $M_{max;min}$) were normalised to the greenfield values ($N_{max\,g}$; $M_{max;min\,g}$) in order to give a better picture of the forces variations (equations 6.1 and 6.2). In those, N_{max} is the maximum axial force computed in the presence of the wall, and $N_{max\,g}$ is the value obtained in the greenfield model; $M_{max;min}$ is the maximum/minimum bending moment computed, and $M_{max;min\,g}$ relates to the greenfield model value.

$$\frac{N_{max}}{N_{max\,g}} \tag{6.1}$$

$$\frac{M_{max;min}}{M_{max;min\,g}} \tag{6.2}$$

Table 6.2 presents the embedded wall parameters that were varied and employed during the parametric study. In that, five possible relative distances of the embedded wall toe, h, to the centre of the tunnel were adopted: tunnel crown (h=-0.5Dt); tunnel axis (h=0.0Dt); tunnel invert (h=0.5Dt); tunnel invert plus 0.75Dt (h=0.75Dt); tunnel invert plus 1.0Dt (h=1.0Dt). Additionally, five possible offsets, d, from the embedded wall to the tunnel axis were assumed. To be simplified, the offset is presented normalized by the tunnel diameter (d/Dt).

Figure 39 illustrates the scheme adopted during the parametric study. The embedded wall thickness, t, assumed values of: 0.4m; 0.6m; 1m. Also, it was explored the use of a sheet pile wall (AU20) (ArcelorMittal, 2019). It is worth mentioning that the roughness interface assumed for the embedded wall was 0.6ϕ, while for the sheet pile was 0.3ϕ. The flexural rigidity of each embedded wall is described in Table 6.2.

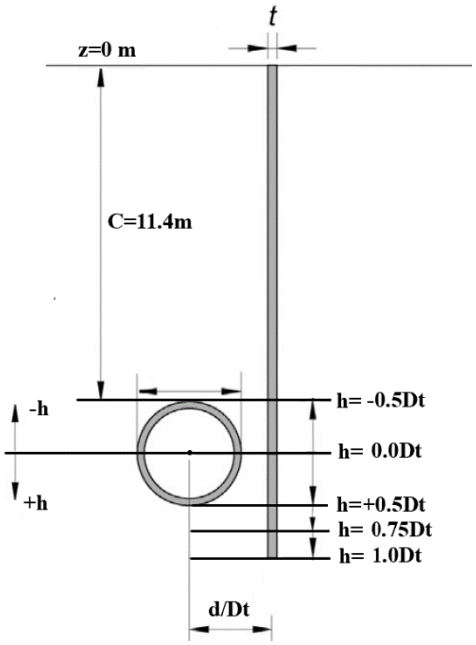

Figure 39-Representation of the relative depth to the tunnel (h) centre of the embedded wall (adapted from Rampello et al., 2019).

Table 6.1- Characteristics of the wall in the parametrical study.

h	Normalised Offset (d/Dt)	Thickness-t (m)
"-0.5Dt; 0.0Dt; 0.5Dt; 0.75Dt; 1.0Dt	0.75; 1; 1.25; 2.0; 3.0	0.4; 0.6; 1.0; Sheet Pile(AU20)*

Table 6.2- Flexural rigidity for different embedded walls.

	Sheet pile wall	Concrete wall		
	AU20(*)	**t=0.4 m**	**t=0.6 m**	**t=1.0 m**
EI **(N.m^2/m)×10^6**	88.88	159.9	540	2490

(*)Arcelor Mittal catalogue; EI-flexural rigidity; t-thickness

6.2 Influence of the location and depth of the embedded wall

The influence of the location and of the relative depth of the embedded wall was explored by a set of thirty FE numerical analyses. The parameters that were changed during this parametric

study are described previously (see Table 6.1). In this study, the thickness remained constant (t=0.4m) (Figure 39).

6.2.1 Efficiency parameters of the embedded wall

Another aspect analysed in this section was the wall embedment length in the AP formation. The settlement of the wall could be related to the rigidity of the material where the wall is embedded. As a result, the efficiency parameters of the embedded wall could be affected by this relative stiffness difference (AP formation and AE formation). The respective embedment heights of the wall are described in Table 6.3 for distinct h, and (d/Dt). In the case of h≤0.0Dt, there was no wall embedment in the AP formation, regardless of its offset from the tunnel axis,d.

Table 6.3- Embedment height(m) of the wall in the AP formation for distinct offset distances.

Offset(d)	0.75Dt	1Dt	1.25Dt	1.5Dt	2Dt	3Dt
h=0.5Dt	1.82	1.21	0.58	0	0	0
h= 0.75Dt	3.64	3	2.39	1.79	0.71	0
h=1Dt	6.06	5.43	4.82	4.22	3.14	1.33

Figure 40 shows the rate at which the global efficiency varied with the embedded wall normalized offset distance. This graph aims to give a better picture of the problem and compares the performance of the wall for distinct h and d/Dt. In that, each line with distinct colours corresponds to different relative distances to the tunnel centre. Overall, there was a decreasing trend of the global efficiency rate as the offset distance increases. The results suggest that short walls (h≤0.0Dt) seem to be ineffective in changing the volume of the settlement trough, irrespective of the offset distance. On the other hand, longer walls (h≥0.5Dt) attained higher global efficiency rates, a maximum of 51%, when d/Dt=0.75. However, it is worth noticing that for embedded wall with h≤0.5Dt, the global efficiency sharply decreases, around 23%, from d/Dt=1 to d/Dt= 1.25. This behaviour may be justified due to the embedment height decrease (from 1.21m to 0.58m) in the AP formation. The same justification could be given about the global efficiency rates between embedded walls with h=0.75Dt at d/Dt=1, when it increases to d/Dt= 3 (no embedment height is observed in the AP formation). In summary, the global efficiency rates are likely to decrease from 51% (h=1.0Dt; d/Dt=0.75) down to zero when the embedded wall moves away from the tunnel axis, which approximates the problem to greenfield model.

It is worth noting that embedded walls (h≥0.5Dt; d/Dt≤1) attained similar global efficiencies irrespective its relative distance to the tunnel centre. Thus, increasing the wall height in the model will not necessarily increase the global efficiency.

The negative efficiency rates obtained for short embedded walls (h=-0.5Dt) suggests that the volume of the settlement trough was increased. Thus, the effect of the wall is detrimental to the problem; however, this effect seems to be negligible. One reason that could explain this is that the embedded wall moves together with the ground movement since they are less "stable" for having no continuity in depth.

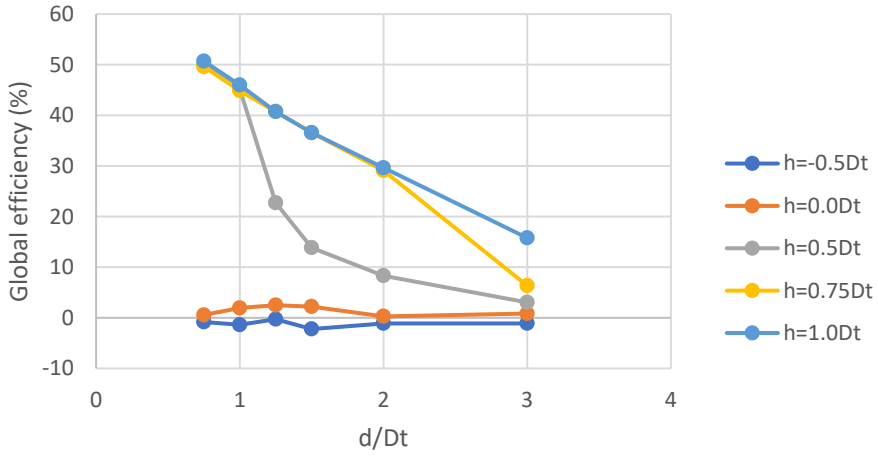

Figure 40- Influence of the relative depth to the tunnel centre in the global efficiency at distinctive offset distances.

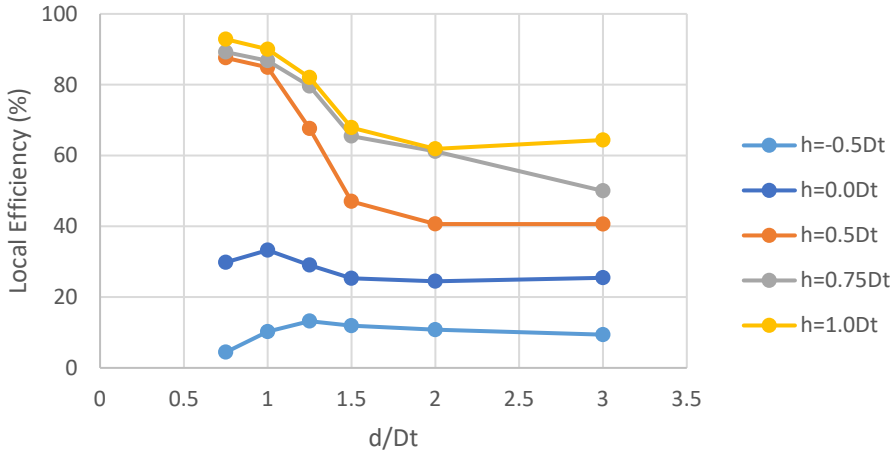

a)

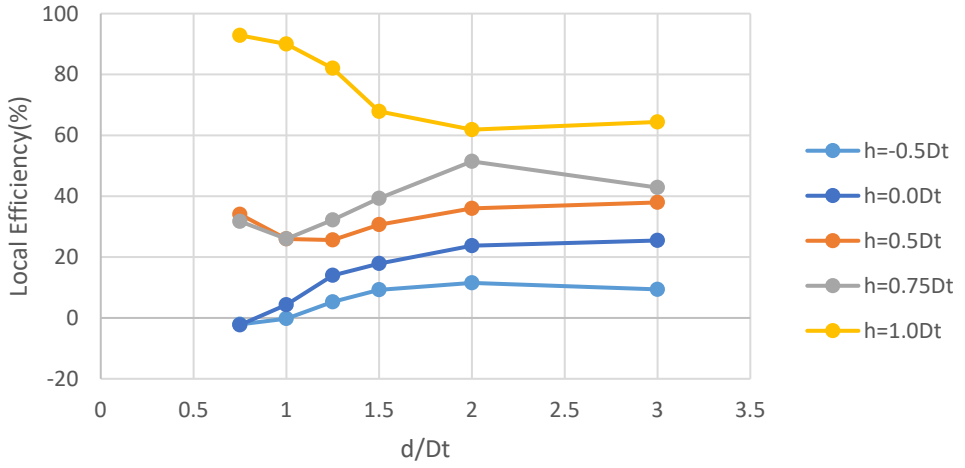

b)

Figure 41- Local efficiency: a) behind ; b) in front of the wall.

The local efficiency rates behind and in front of the embedded wall for the same set of numerical analyses are plotted in Figure 41a)b), respectively. Overall, there was a positive effect of the embedded wall, with a reduction of the settlements behind and in front of the wall. The results from Figure 41a) shows that short embedded walls (h≤0.0D) have a negligible effect in reducing the settlements behind the embedded wall. The maximum local efficiency rate computed was not greater than 34% for h≤0.0Dt, irrespectively to the embedded wall offset distance. Contrarywise, longer walls (h≥0.5Dt) have a positive effect in reducing the settlement behind the wall up to 92.85% when d/Dt=0.75. It is of interest to note that the embedment height in the AP formation (see Table 6.3), affects the local efficiencies behind the wall, which are nearly identical for longer embedded walls (h≥0.5Dt) at the same offset distance (d/Dt≤1). However, this behaviour tends to change when the embedment height is reduced in the AP formation (h=0.5Dt; d/Dt=1.25). One aspect that is worth mentioning is the substantial increase (front) and a levelling off (behind) of the local efficiency rates when the wall moves away from the tunnel (in front of the embedded wall; h≤0.75Dt), even irrespectively of the embedment in the AP formation. One reason for this could be related to wider settlement trough.

In conclusion, longer embedded walls (h=1Dt) attained larger local efficiency rates than the shorter embedded walls.

6.2.2 Effects on the tunnel lining

Figure 42a) illustrates the variations of the axial forces acting on the lining as a function of the embedded wall normalized offset distance. In that, each line relates to distinct relative depths to the tunnel centre, h. The comparison between the axial forces in greenfield and in the presence of the embedded wall reflects that the changes in the ground stress are irrelevant (≤2.5%) irrespectively the offset distance and relative depth.

Figure 42b)c) shows the variations of maximum and minimum the bending moments acting on the lining as a function of the embedded wall normalized offset distance. In that, each line relates to distinct relative depths to the tunnel centre, h. The comparison between the initial bending moments (greenfield and in the presence of the wall) reflects that the changes in the maximum and minimum bending moments are up to 24% when d/Dt=0.75 for h=0.5Dt. One reason that could explain why a shorter embedded wall (h=0.5Dt) presents smaller minimum bending moments in the tunnel than could be related to the larger number of yielding elements around the lining, at the AP formation (h=0.5Dt; h=0.75Dt), as displayed in Figure 43a)and b) for h=0.5Dt and h=1.0Dt, respectively.

Overall, the given results reflect that when the embedded wall moves away from the tunnel axis, the forces acting in the lining approximates to the greenfield (d/Dt≥2), irrespectively of h.

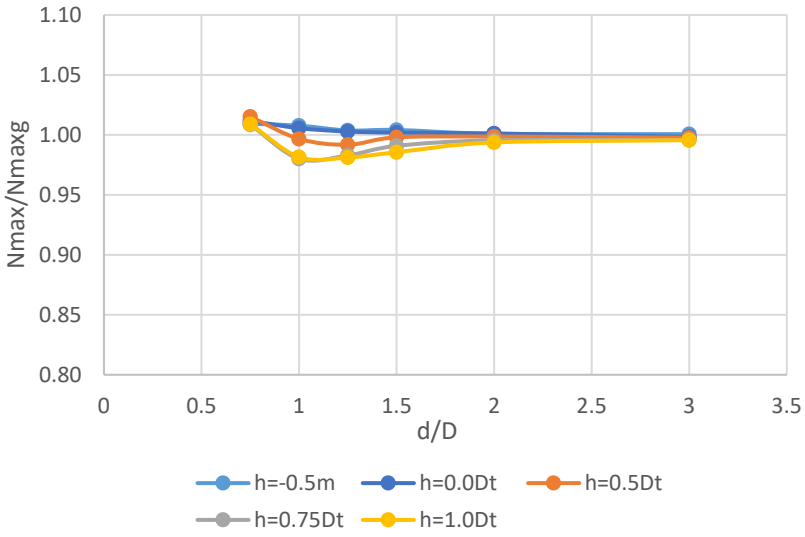

a)

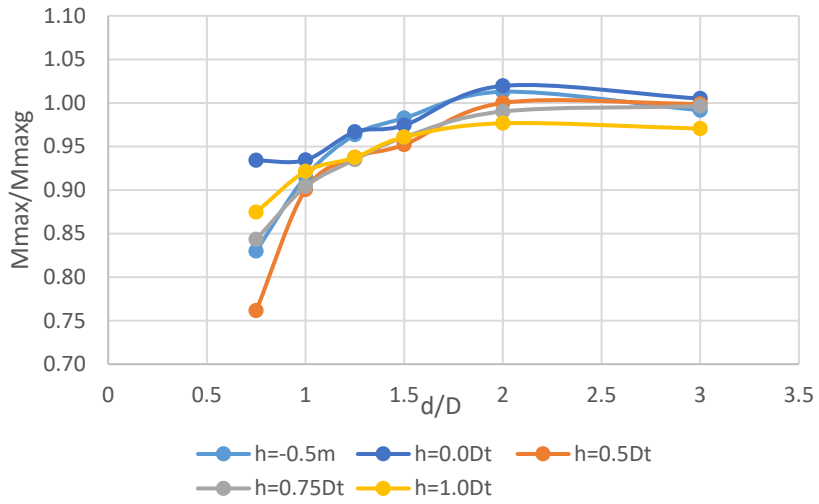

b)

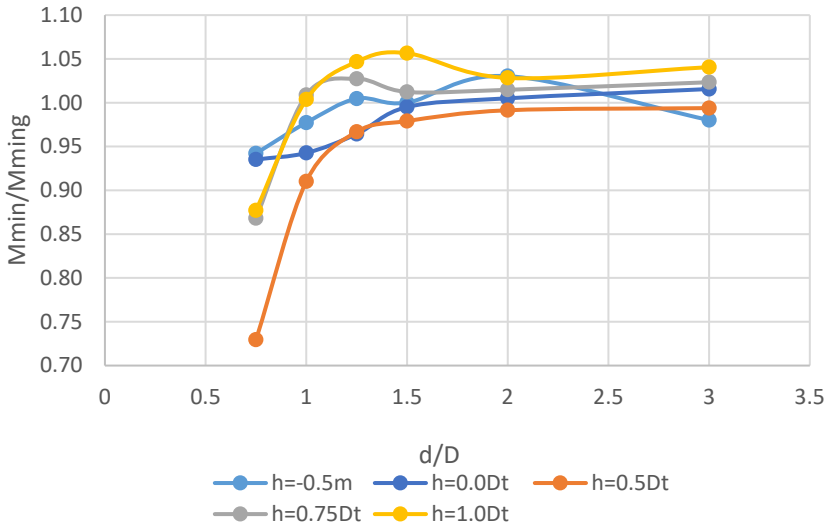

c)

Figure 42-Changes of the normalised forces mobilised in the lining with the embedded wall at different relative depths and correlated with greenfield model: a) axial forces; b) maximum bending moment; c) minimum bending moment c).

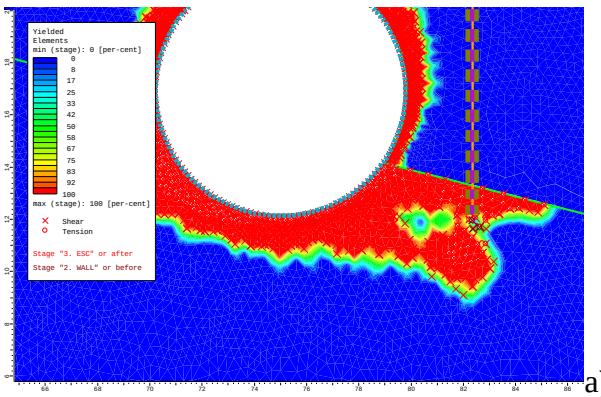

a)

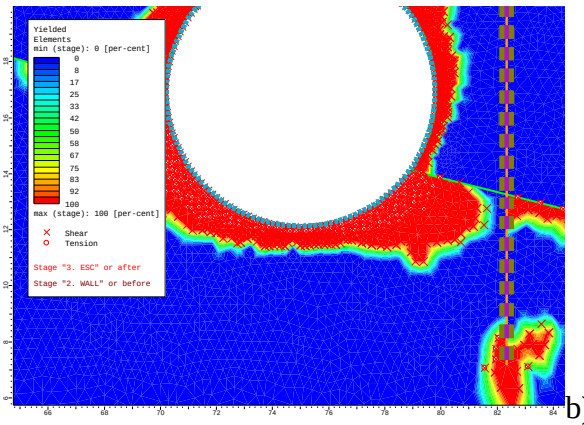

b)

Figure 43-Comparison between the yielded elements zone: a) h=0.5Dt; d/Dt=0.75 b) h=1.0Dt; d/Dt=0.75.

6.2.3 Effects on the wall

The distribution of the bending moments and axial forces acting on the wall is plotted in Figure 44a), b) and c) as a function of its offset distance. Each line relates to distinctive relative depths to the tunnel centre. In Figure 44a) and b), it is possible to note that the development of the maximum and minimum bending moments is higher for longer walls (h=1.0Dt) at a small distance from the tunnel axis (d/Dt=0.75). In general, from the inspection of Figure 44, the maximum and minimum bending moments tends to rise from 28.34kN.m/m to 143.31kN.m/m and from -52.51kN.m/m to -128.66kN.m/m (h=1.0Dt) when the wall approaches the tunnel. This behaviour may be explained due to ground load transfer that develops after the excavation and around the tunnel (i.e.ground arch effect) acting on the embedded wall. Also, it may be related to the embedment of longer walls in the AP formation (fixed restrain), which causes minimum bending moment peaks of around 91 kN.m/m (h=0.5Dt; h=0.75Dt; h=1.0Dt) located at the AE formation. It was not possible to justify the reason for the bending moment peak (h=1.0Dt; d/Dt=2)

In Figure 44c), the maximum axial forces on the embedded wall also increase from 696kN/m to 957kN/m (h=1.0Dt). It is worth noting that the differences between the lines of the axial forces are related to the gravity forces since longer embedded walls are heavier than short walls. Additionally, when the embedded wall moves away from the tunnel, the embedded wall is less affected by the ground load transfer (ground arch effect) which approximates to its self-weight of 249.2kN/m (h=1.0Dt;d/Dt=3).

The increasing trend of the axial forces acting on the embedded wall when it approximates to the tunnel may be related to the arch effect induced by the excavation. Thus, it is possible to infer that the stresses mobilised on the wall are higher for longer walls.

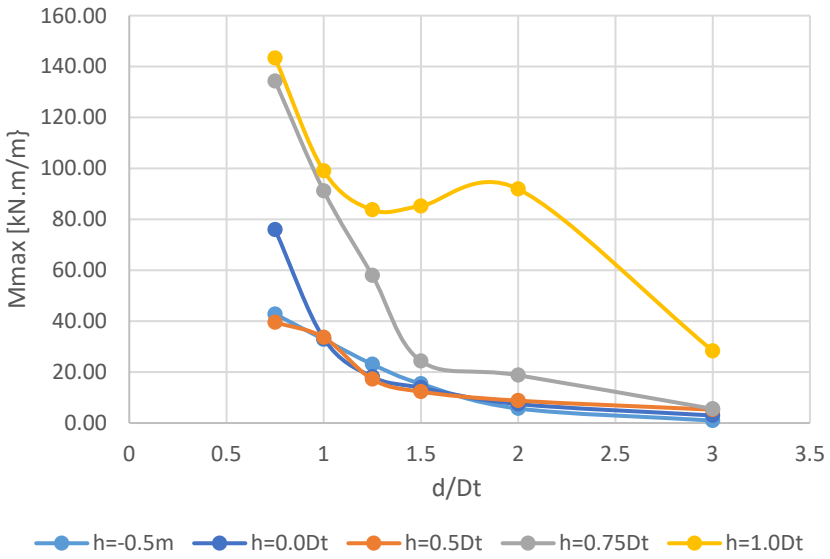
160.00
140.00
120.00
100.00
80.00
60.00
40.00
20.00
0.00
Mmax [kN.m/m]
0
0.5
1
1.5
2
2.5
3
3.5
d/Dt
h=-0.5m
h=0.0Dt
h=0.5Dt
h=0.75Dt
h=1.0Dt

. a)

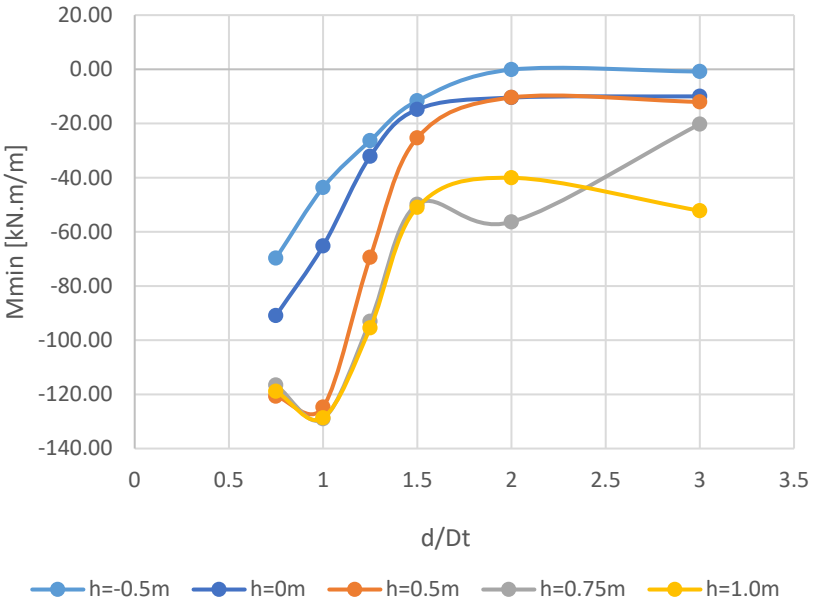
20.00
0.00
-20.00
-40.00
-60.00
-80.00
-100.00
-120.00
-140.00
Mmin [kN.m/m]
0
0.5
1
1.5
2
2.5
3
3.5
d/Dt
h=-0.5m
h=0m
h=0.5m
h=0.75m
h=1.0m

b)

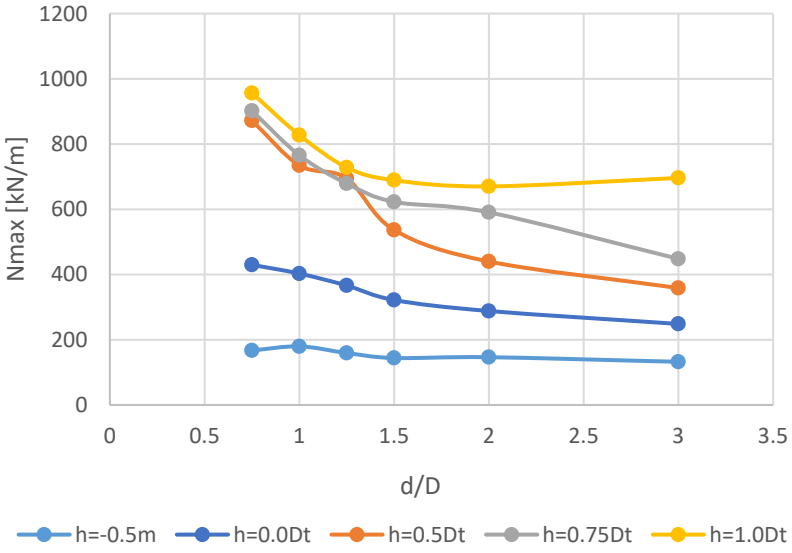

c)

Figure 44- Stresses mobilised in the wall after the tunnel excavation: a) maximum bending moments; b) minimum bending moment; c) axial forces.

6.3 Influence of the stiffness of the embedded wall

The influence of the stiffness of the embedded wall was investigated by a set of twenty-four FE numerical analyses. In that, five possible stiffnesses were assumed (see Table 6.2), for six distinct offset distances (d/Dt=0.75;1.0;1.25;1.5;2.0;3.0). The parametric study was carried out with concrete embedded walls (t=0.4;0.6;1.0) and an AU20 sheet pile wall (ArcelorMittal, 2019). Table 6.4 presents the mechanical and geometrical properties of the sheet pile wall. The idea of using a sheet pile wall was to investigate a different solution (very flexible) and with a smoother interface instead of rough concrete walls. It is worth mentioning that the relative depth to the tunnel centre, h, was maintained constant (h=0.75Dt), irrespectively of the stiffness and of the offset distance from the tunnel.

Table 6.4-Geometrical and mechanical properties from the Pile Sheet AU20

Pile AU20	
E(GPa)	200
t (mm)	12
Sectional area(cm2/m)	165
γ(kN/m3)	78
ν	0.3

6.3.1 Efficiency parameters of the embedded wall

Figure 45 shows the development of the global efficiency rate for the different offset positions of the embedded wall. Overall, the analysis of the chart shows a decreasing trend of the global efficiency rate as the offset distance increases. The results also indicate that the influence of stiffness in the global efficiency rate seems to be nearly zero, except for the pile sheet wall when d/Dt=0.75. At this distance, the pile sheet wall attains 41% of global efficiency, while the concrete walls attain up to 50%. One reason for this could be that the smooth interface of the sheet pile has a significant influence on global efficiency parameter when the embedded wall is close to the tunnel (d/Dt=0.75). In the case of the wall is installed for normalised distances greater than 3, the wall appears to be ineffective. Hence, the stiffness seems to be irrelevant when computing the global efficiency.

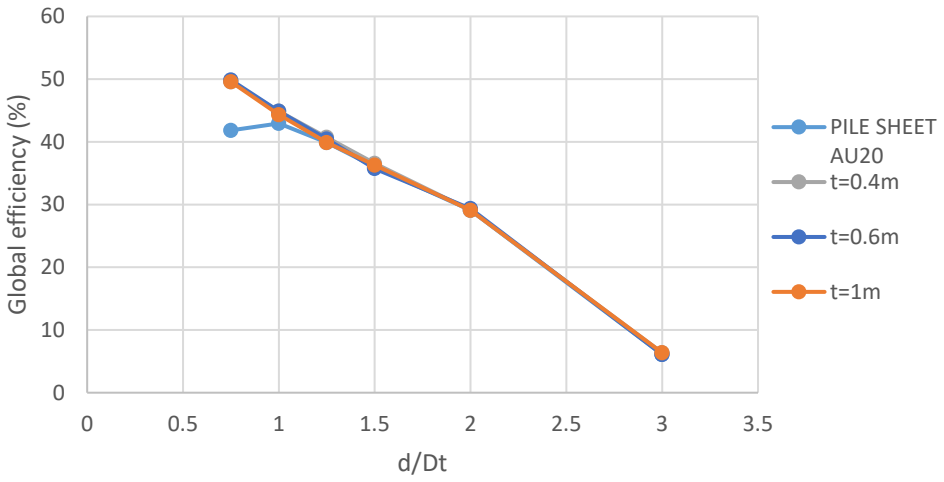

Figure 45- Global efficiency rates for walls with distinctive stiffness.

In Figure 46a) and b), the local efficiencies computed against the offset distance are plotted. The results suggest similar local efficiencies behind the wall regardless of the stiffness values, ranging from 84% (t=1m;d/Dt=0.75)), and 95% for the pile sheet wall (same position). However, when d/Dt=3 for the pile sheet wall, the local efficiency computed behind the wall attains only 23%, compared to 50% from the other walls.

From Figure 46b), it is possible to note a negative local efficiency rate (-18.27%) computed in front of the wall for the sheet pile wall installed at 0.75Dt. This result means that the pile sheet wall increases the settlement in front of the wall, which is an undesirable effect. In the case of stiffer walls, the computed local efficiency rates suggest a positive effect of the wall, up to 52.52%(t=1.0m; d/Dt=2). These results could be related to the stiffness and also to the

roughness interface, which is smoother for the sheet pile wall when compared to the concrete embedded walls.

Overall, the embedded wall had a positive effect on reducing local settlements around it, except to the pile sheet wall that increased the settlements in front of the wall in about 18% for d/Dt=0.75.

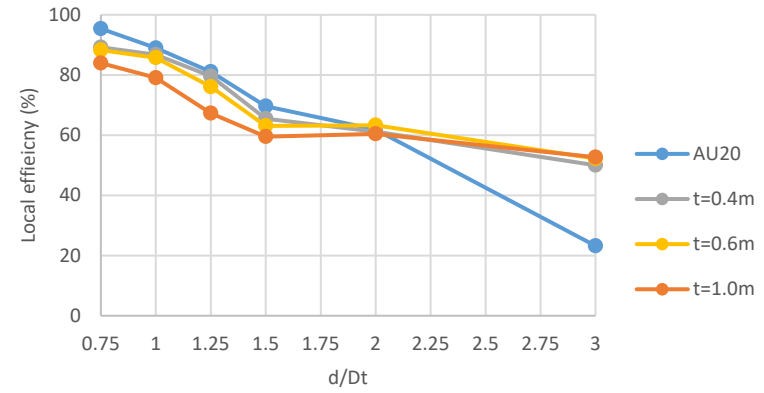

a)

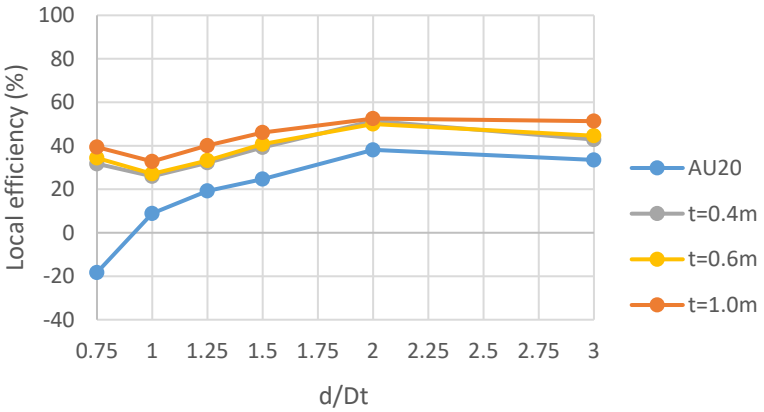

b)

Figure 46- Local efficiencies computed for different stiffness values: a) behind the embedded wall; b) in front of the embedded wall.

6.3.2 Effects on the tunnel lining

Figure 42a),b) and c) illustrate variations of the forces acting on the lining as a function of the embedded wall offset distance. In this case, it was explored the influence of changing the embedded wall stiffness on the existing linning at different offset distances, where each line relates to distinct stiffness.

From Figure 42a), it is possible to observe a negligible effect again (<2.5%) in the presence of the embedded wall on the axial forces acting on the lining, irrespectively the offset distance and the stiffness change. The axial forces increase less than 1% (Depth=0.75Dt) and decrease less than 2.5%(t=1%;d/Dt=1). These results show that the variations in the axial forces are irrelevant regardless of the flexural stiffness.

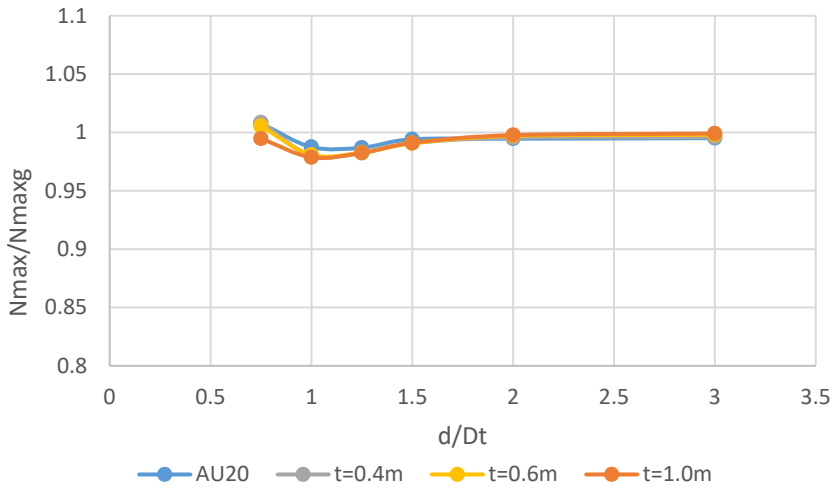

a)

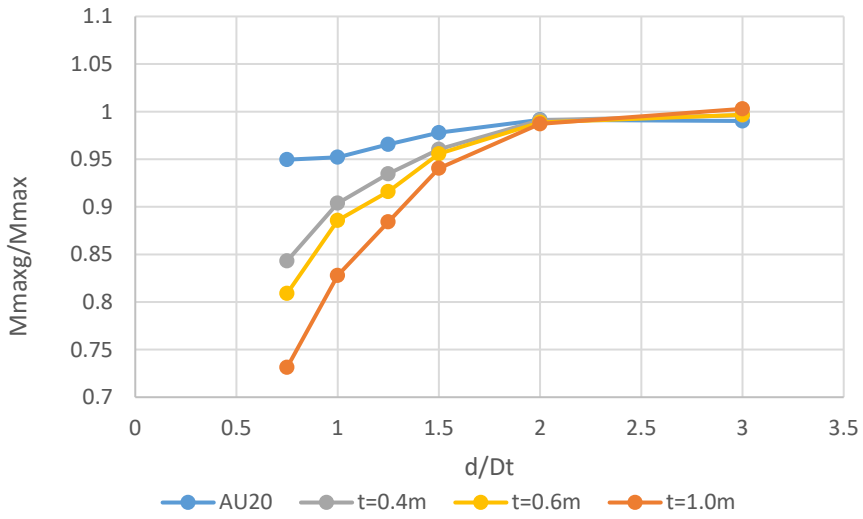

b)

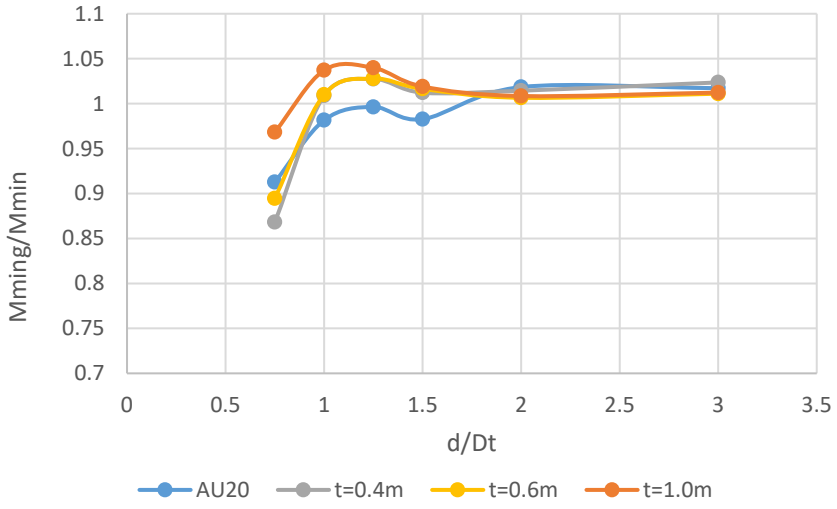

c)

Figure 47- Changes of the normalised forces mobilised in the tunnel lining after the installation of the embedded wall depth=0.75Dt correlated with normalised greenfield conditions for distinctive stiffness: a) axial forces; b) maximum bending moment; c) minimum bending moment.

Figure 47b) and c) plots the normalised maximum and minimum bending moments acting on the tunnel lining. The evolution of the maximum bending moments suggests that stiffer embedded walls (t=1m) are capable of reducing more the maximum bending moments, which occurs in the AP formation, in the tunnel lining, up to 27% (d/Dt=0.75). In the case of the wall is d/Dt≥2, this effect is negligible. The development of the minimum bending moment curves suggests that when the embedded wall moves closer to the tunnel, there is a downward trend of the minimum bending moments, regardless of its flexural stiffness. The maximum reduction of the minimum bending moment is about 13% (d/Dt=0.75; t=0.4m).

6.3.3 Effects on the wall

The distribution of the maximum bending moments and axial forces acting on the embedded wall as a function of the offset distance is plotted in Figure 48a),b) and c). In these, each curve relates to the stiffness variations. In Figure 48a) is possible to observe that differences between the lines are due to the gravity forces (the thicker the embedded wall, the higher axial forces are mobilised). In addition to that, as the embedded wall gets closer to the tunnel, the axial force increases substantially, from 597.3kN/m (t=1.0m;d/Dt=3) to 1097.05kN/m (t=1.0m;d/Dt=0.75). One reason for that could be the influence of the ground arch effect during the tunnel excavation. It is worth mentioning that the sheet pile wall had only a slight increase in the axial forces when it gets closer to the tunnel, which could be related due to its smooth interface.

The maximum bending moment (231.39kN.m/m) develops at d/Dt=1 for the stiffest embedded wall (t=1.0m) at the AP formation (Figure 48b))It increases from 0 kN.m/m (all embedded walls) to a maximum value of 231kN.m/m (t=1m). The reason for this peak could be related to the minimum moment developed in the transition zone between the fill/alluvial layer and the AE formation. However, it decreases when the embedded wall is at d/Dt=0.75, which could be justified due to the increase of the embedment height in the AP formation. In the case of the embedded wall is d/Dt=3, it does not have any impact from the tunnel excavation, irrespectively to its stiffness, with the exception for the minimum bending moment., where even at d/Dt=3, the embedment height is still 1.33 m.

The distribution of the minimum bending moments is plotted in Figure 48c). It can be seen that the minimum value for the stiffest embedded (t=1m) wall was as impressive -516.96kN.m/m, developed at the tunnel springline depth. This behaviour observed could be related to the ground arch effect, which is more intense closer to the embedded wall. The closer the embedded wall is, more forces will be acting on it

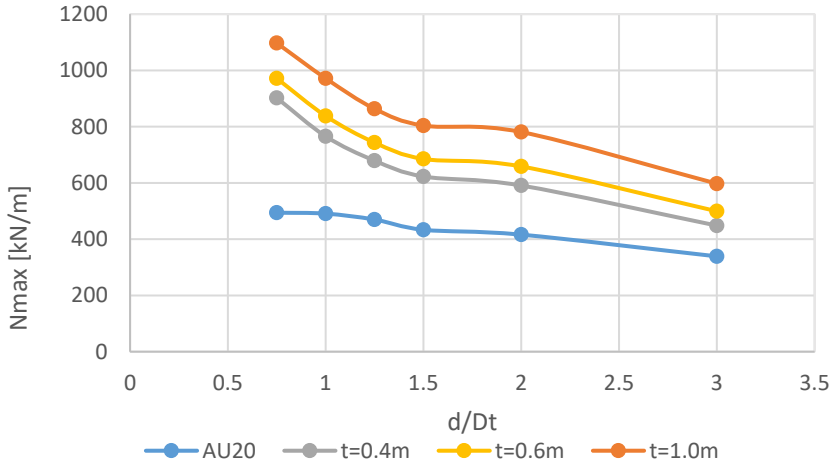

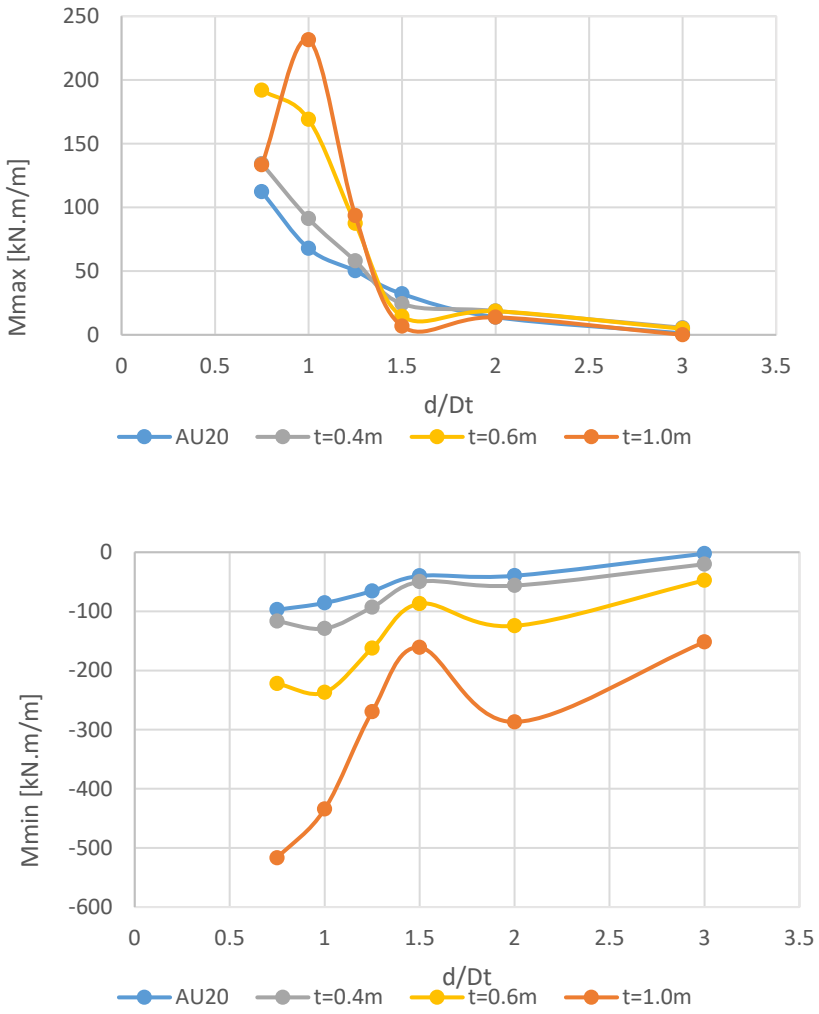

Figure 48- Forces mobilised in the embedded wall after the tunnel excavation for distinctive stiffness: a) maximum bending moments; b) Minimum Bending Moment; c) Axial forces.

6.4 Influence of the stress relief factor – Case of Section P10A

The influence of the stress relief factor, α, was investigated by a set of twelve FE numerical analyses. The parameters assumed for the embedded wall were: t=0.4; h=0.75Dt; and for its offset distance varied (d=0.75Dt; 1.0Dt; 1.25Dt; 1.5Dt; 2.0Dt; 3.0Dt) (see Figure 39) . It is worth noting that sections P9 and P10A were simulated for different α values (see Table 6.5), thus, there is an interest to assess how this change affects the lining, the embedded wall, and the efficiency parameters.

Table 6.5- Stress relief factors and the Volume of the settlement trough Va attained in FE.

	α	Va(%)
P10A	0.41	2.69
P9	0.789	3.61

6.4.1 Efficiency parameters of the embedded wall

Figure 49 illustrates the rate at which the global efficiency varied with the embedded wall normalised offset distance for distinct values of α 0.789 and 0.41 (sections P9 and P10A, respectively). This graph aims to give a better picture of the influence of α in the problem, by comparing the global efficiency parameters. In that, each line with a distinct line corresponds to section P9 and P10A. In general, there was an expectable decrease, in the global efficiency rate as the embedded wall moves away from the tunnel. The given results show a larger global efficiency rate of the embedded wall for section P10A compared to section P9, up to 13.62% (d/Dt=0.75). One reason for this is that the reference volume of the settlement trough Va from section P9 (3.61%) is higher than the volume in section P10A (2.61%)(see Table 6.5). The maximum efficiency rate attained was around 49.58% for section P9, while for section P10A the wall attained 63.2% for d/Dt=0.75. Therefore, it is suggested that higher values of α leads to smaller global efficiency rates for this problem. However, it is required to investigate for more different values of α to make this conclusion for different soil stratigraphies.

In cases that the embedded wall is far from the tunnel (d/Dt>3.0), the embedded walls seem to be ineffective in changing the volume of the settlement trough.

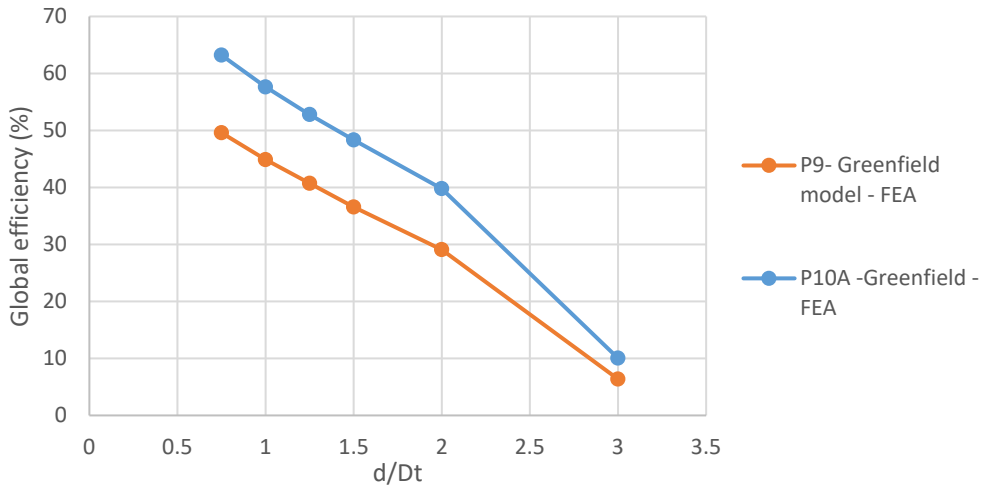

Figure 49-Global efficiency rates computed for sections P9 and P10A.

The local efficiencies rates computed behind and in front of the embedded wall are plotted in Figure 50a)b). The results show, in general, a slight decreasing trend of the local efficiency rates computed in front and behind the wall with the increase of the offset distance (except for section P9 in front of the embedded wall). The local efficiency rate behind the wall attained its maximum of 92.90% for section P10A, and 89.21% for section P9 (d/Dt=0.75), while its minimum attained 58.21% and 50%, respectively (d/Dt=3) (see Figure 50a)). Similarly, the computed local efficiencies in front of the wall attained its maximum of 79.15% for section

P10A and 31.73% for section P9, while its minimum attained 58.21% and 42.86% (Figure 50b)). From the charts described, it is possible to conclude that for higher values of the stress relief factor, the local efficiency tends to decrease irrespective of the normalised offset distance.

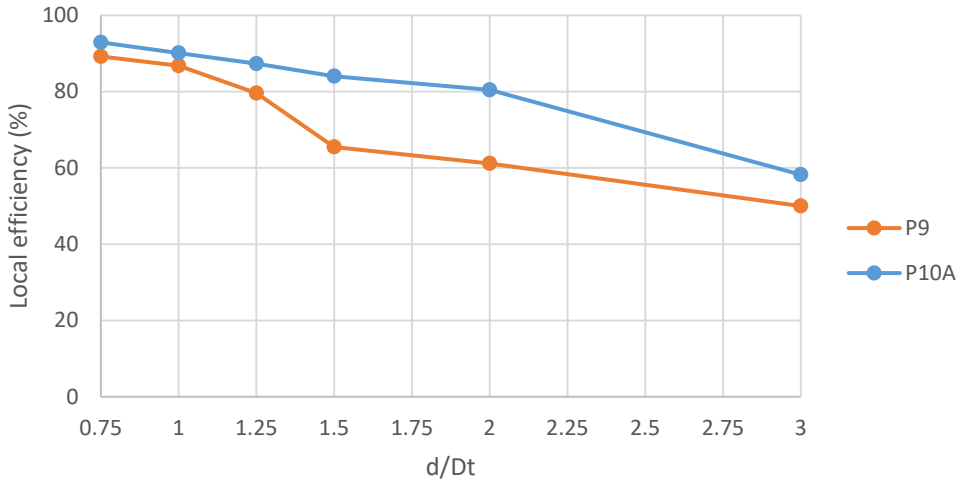

a)

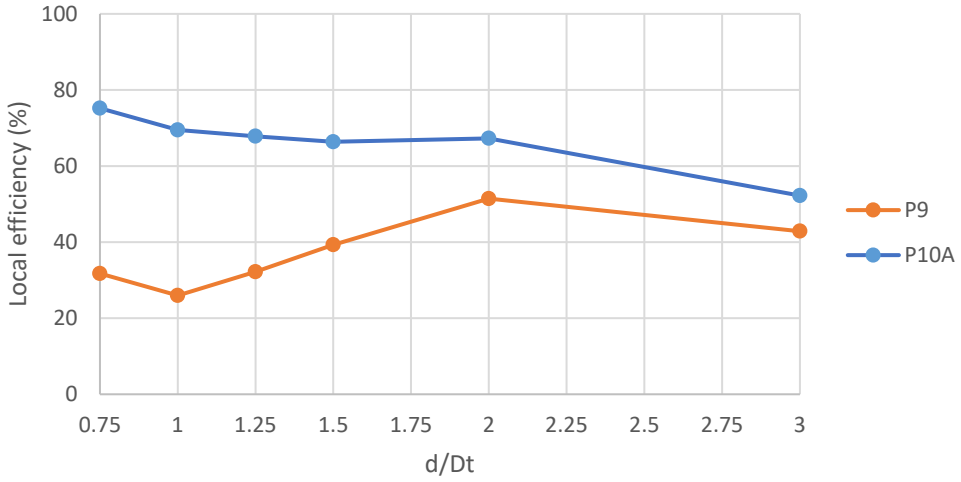

b)

Figure 50- Local efficiencies computed for sections P9 and P10A: a) behind the embedded wall; b) in front of the embedded wall.

6.4.2 Effects on the tunnel lining

Figure 51a);b) and c) depicts the variations of the forces acting on the lining of the tunnel as a function of the embedded wall offset distances. In that, each curve relates to distinct parameters α, which are related to the greenfield forces acting in the lining (section P10A) (see Table 6.5). The maximum axial forces acting in the lining are illustrated in Figure 51a). The computed

results suggest an irrelevant impact of the embedded wall in the axial forces in the lining, irrespectively of the parameter α (<2.5 %; d/Dt=0.75).

In Figure 51b), the differences in the curves suggest a negligible impact of the parameter α in the maximum bending moments (<2%; d/Dt=0.75). Meantime, the comparison of the minimum bending moment computed for a distinct α, shows a negligible differences (<5%) between the forces mobilised in the lining in the presence of the embedded wall (d=0.75Dt).

Overall, the computed results suggest a negligible impact of the parameter α, in reducing or increasing the forces mobilised in the lining of the tunnel in the presence of the embedded wall. However, further analyses are required to prove, in fact, this suggestion.

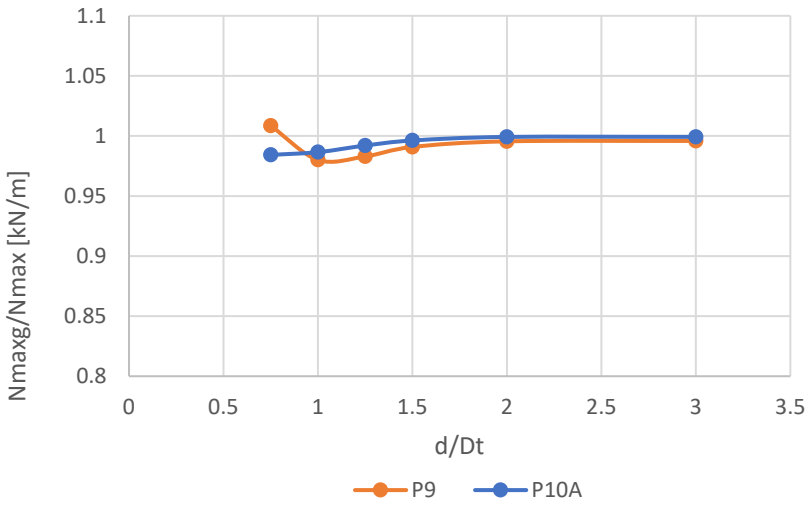

a)

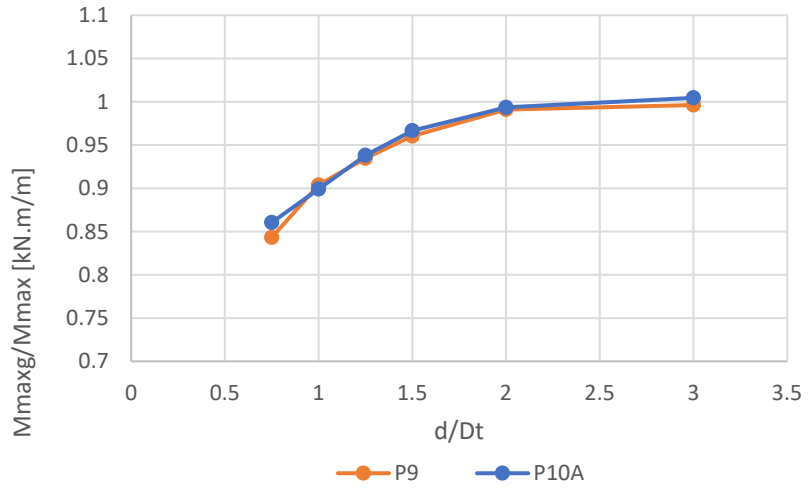

b)

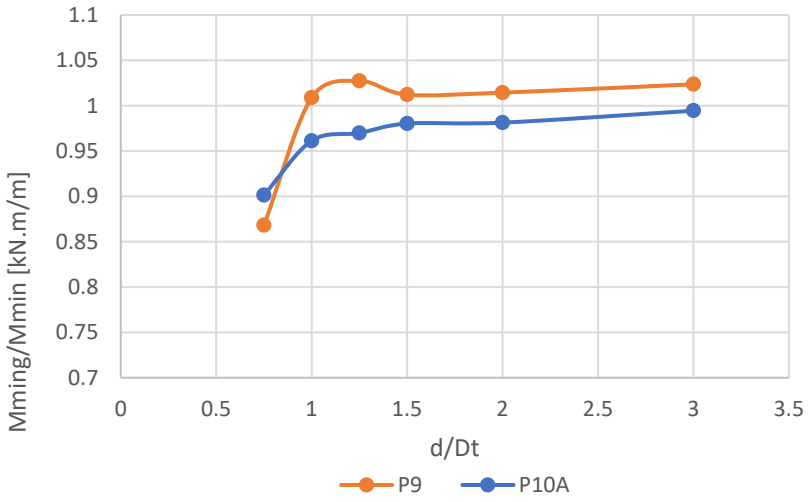

c)

Figure 51- Changes of the normalised forces mobilised in the tunnel lining after the installation of the embedded wall at different depths correlated with greenfield conditions: a) axial forces; b) maximum bending moment; c) minimum bending moment.

6.4.3 Effects on the wall

Figure 52a),b) and c), illustrates the variations of the forces acting on the embedded wall as a function of its offset distance. Each curve relates to distinct α (sections P9; P10A).

Figure 52a) depicts the development of the axial forces acting on the embedded wall. It is worth noting that the embedded wall self-weight is around 225.88kN/m. Thus, the given results suggest when the embedded wall moves away from the tunnel, the axial forces tends to be only affected by gravity forces, since it approaches its self-weight (d/Dt=3; 451 kN/m). The comparison between each curve (P9 and P10A) suggests that the embedded wall was more loaded in section P9 (higher α). One reason that could justify that is the larger movements induced in the ground around the tunnel in section P9 since the ground had a higher stress relief factor. The maximum differences in the axial forces were around 225kN/m (d/Dt=0.75). However, when the embedded wall moves away, this effect (distinct α) tends to be less significant.

Figure 52b) shows the variations of the maximum bending moments along the embedded wall. The results suggest a negligible influence of the α parameter for normalised offset distances greater than d/Dt=1.25. However, when the embedded wall approximates to the tunnel axis, the difference between the bending moments are larger, 134 kN.m/m and 94.48 kN.m/m, for sections P9 and P10A, respectively. One reason that could explain that could be related to the larger movements induced by the excavation due to the ground arch effect and the embedment

height in the AP formation, which approximates to a fixed restrain as embedment height increases when the wall moves closer to the tunnel. The same effect was seen for minimum bending moments, as shown in Figure 52c). The maximum differences between the minimum bending moments for sections P9 and P10A are around -65.42 kN.m/m (d/Dt=1). When the embedded wall moves away from the tunnel axis, this difference seems to be insignificant (d/Dt=1.25)

Overall, it is suggested that the embedded wall is more loaded when it approximates to the tunnel and when the α parameter increases due to the arch effect.

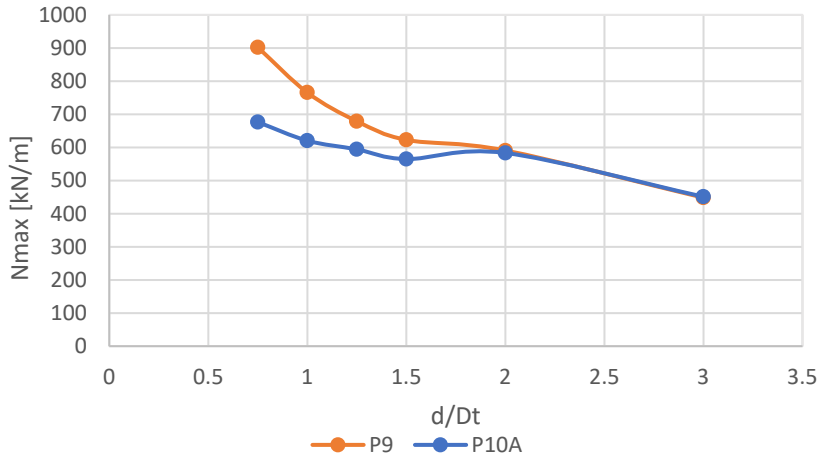

a)

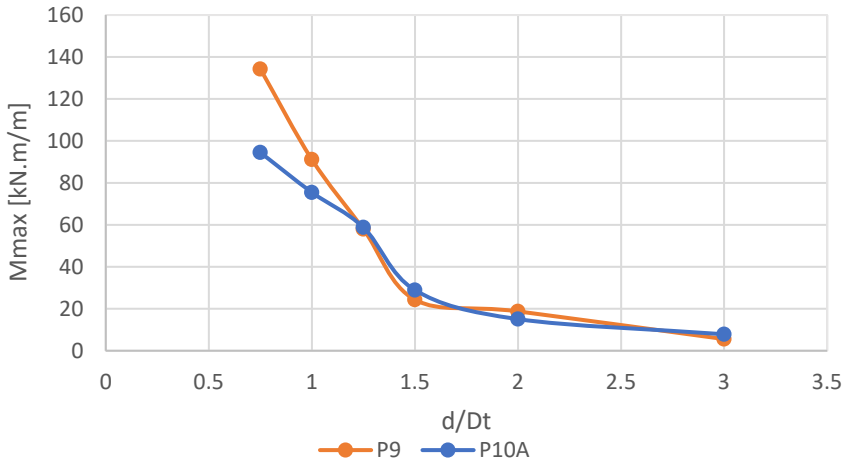

b)

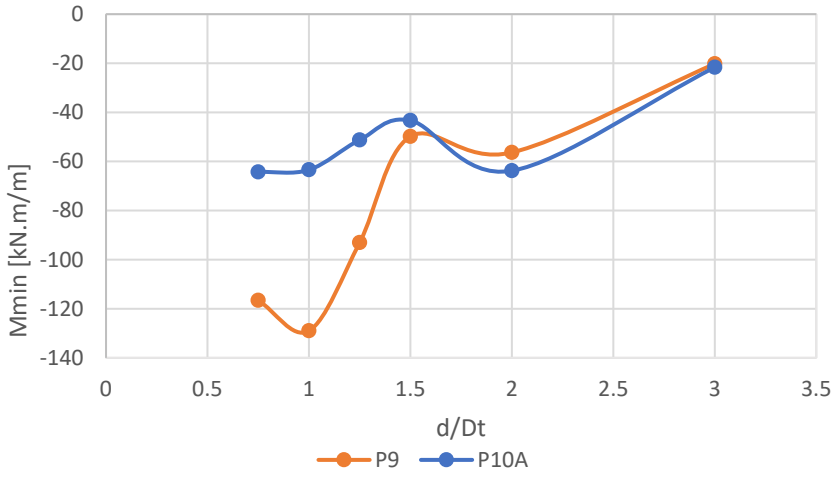

c)

Figure 52- Forces acting on the embedded wall after the tunnel excavation for sections P9 and P10A: a) axial forces; b) maximum bending moments; c) minimum bending moment.

7 CONCLUSIONS AND FURTHER WORKS

7.1 Conclusions

There are some mitigation measures, such as strengthening of the ground; compensation grouting; physical barriers that can be adopted in order to minimise the magnitude of these movements on the surface. In this project, a continuous embedded wall was installed prior to the tunnel excavation and aside of it. The aim is to produce a discontinuity on the ground and reduce the magnitude of settlements on the surface, and the volume of the settlement trough. However, this soil-structure interaction is dependent on the embedded wall location and characteristics, which can affect the volume of the settlement trough and the displacements around it. The influence of the embedded wall on the forces acting on the lining is investigated, as well the forces acting along with the embedded wall depth.

The problem was investigated by performing several numerical analyses in plane-strain conditions. In that, a total of sixty-six finite element analyses were carried out. Having as a reference the case of Section 63 of the Green Line of the Lisbon Metro network, the calibration of the model was based on the settlements measured in the field (instrumented sections P9 and P10A), by using the stress relief method. The reason for choosing this specific case was due to excessive settlements measured in the field. Thus, a parametric study was performed to explore how distinctive embedded wall characteristics could affect the problem. In that, it was investigated the influence of depth, location, and stiffness of the embedded wall. The influence of the stress relief factor on the performance of the embedded wall was also explored. In order to assess the embedded wall's efficiency in reducing settlements and the volume of the settlement trough two dimensionless parameters, local and global efficiency, were employed.

Observations and remarks:

The following conclusions are based for the specific case of study, the instrumented section P9 and P10A (Section 63 of the Lisbon Metro network), with the particular stratigraphy, and ground conditions presented. Therefore, some suggestions and conclusions may change for other cases of study with distinctive ground conditions. It is of interest to note that the following conclusions are based on the hydraulic properties and boundary conditions adopted in the model.

The influence of the depth and location of the embedded wall:

- In the global efficiency: the embedded wall seems to be positive when it is embedded at least at the tunnel invert depth. In the case the embedded wall is short (embedded at or above the tunnel springline), the effect seems to be insignificant to the problem. When the embedded wall moves away from the tunnel, around one diameter, the global efficiency rates decline linearly.

- In the local efficiency, it is suggested that the embedded wall should be embedded at least on the springline depth of the tunnel. As the embedded wall gets closer to the tunnel, local efficiencies seem to increase linearly.

- Effects on the lining: the presence of the embedded wall has a negligible impact on the maximum axial forces acting on the lining. When the embedded wall moves closer to the tunnel, less than two diameters, there is a significant reduction on the maximum and minimum bending moments acting on the lining, although the magnitude of the bending moments is generally small.

- Effects on the embedded wall: the axial forces and the bending moments increase considerably when the embedded wall approaches the excavation (less than two tunnel diameters).

The influence of the stiffness of the embedded wall:

- In the global efficiency: the flexural stiffness seems to have a negligible influence.

- In the local efficiency: the flexural stiffness seems to be irrelevant, except for a very flexible embedded wall.

- Effects on the lining: the effect of the flexural stiffness changes seems to be irrelevant for the maximum axial forces acting on the lining. The maximum bending moments were reduced proportionally as the flexible stiffness of the wall increased. Contrariwise, this effect was not observed for the minimum bending moments, where flexible

embedded walls reduced more significantly its magnitude. Overall, the impact of the flexural stiffness seemed to be irrelevant.

- Effects on the embedded wall: the forces increase significantly for stiffer embedded particularly for placed less than one and a half tunnel diameter.

Influence of the stress relief factor:

- In the global efficiency: the stress relief factor seems to have a significant impact. Higher values of the stress relief factor seem to affect the global efficiency of the embedded wall negatively. However, more studies are required to investigate this conclusion.

- In the local efficiency: higher values of the stress relief factor resulted in smaller local efficiency regardless of the offset distance to the tunnel. Still, more studies are required to make this conclusion.

- Effects on the lining: the different values of the stress relief factor in the presence of the embedded wall did not have a significant impact on the forces acting on the lining.

- Effects on the embedded wall: higher values of the stress relief factor resulted in higher forces acting on the embedded wall. This effect is even more visible when the embedded wall moves closer to the tunnel.

Overall, it can be concluded that embedded walls can, in fact, be efficient in reducing ground movements and forces on the lining with some limitations. The embedment height of the wall in a stiffer layer could be related to these conclusions aforementioned.

7.2 Further works

The following suggestions can be taken into account in order to develop future research using a different methodology of assessing the benefits of using an embedded wall:

- The efficiency of the embedded wall can be linked to the horizontal strains.

- The risk assessment of a building could be performed in order to assess the category of damage reduction by using an embedded wall.

- The effects of changing the embedded wall's position by inclining it between the tunnel and the existing building can be studied.

- Numerical analysis with a sophisticated constitutive model can improve the predictions and clarify the key parameters that influence the results.

REFERENCES

Addenbrooke, T., Potts, D. & Puzrin, A. (1997) The influence of pre-failure soil stiffness on the numerical analysis of tunnel construction. *Géotechnique*, **47** (3), pp. 693-712

Almeida e Sousa, J. (2019) *Apontamentos das aulas de túneis do DEC-FCTUC(in Portuguese)*

Amaral, M. J. S. (2006) *Análise dos resultados de observação dos túneis do metropolitano de Lisboa*. Master's thesis. University of Porto.

ArcelorMittal (2019) Steel Foundation Solutions - General Catalogue.

Attwell, P. & Selby, A. (1989) Tunneling in Compressible Soils. *Large Ground Movements and Structural Implications", Tunneling and Underground Space Technology*, **4**

Attwell, P. B., Yeates, J. & Selby, A. R. (1986) Soil movements induced by tunnelling and their effects on pipelines and structures.

Bai, Y., Yang, Z. & Jiang, Z. (2014) Key protection techniques adopted and analysis of influence on adjacent buildings due to the Bund Tunnel construction. *Tunnelling and Underground Space Technology*, **41** pp. 24-34

Bilotta, E. & Taylor, R. (2005) Centrifuge modelling of tunnelling close to a diaphragm wall. *International Journal of Physical Modelling in Geotechnics*, **5** (1), pp. 27-41

Bilotta, E. (2008) Use of diaphragm walls to mitigate ground movements induced by tunnelling. *Géotechnique*, **58** (2), pp. 143-155

Breth, H. & Chambosse, G. (1975) London: Pentech Press.

Britto, A. M. & Gunn, M. J. (1987) *Critical state soil mechanics via finite elements.*

Burland, J. (1995) Assessment of risk of damage to buildings due to tunnelling and excavatioins. In *Proceedings of the 1st Int. Conf. on Earthquake Geotech. Engrg., IS-Tokyo'95*.

Burland, J. B., Standing, J. R. & Jardine, F. M. (2001) *Building response to tunnelling: case studies from construction of the Jubilee Line Extension, London.* Thomas Telford.

Chapman, D. N., Metje, N. & Stark, A. (2017) *Introduction to tunnel construction.* Crc Press.

Chen, X., Liu, Y., Cao, W. & He, Z. (1998) Protection for the former observatory during construction of the Yan An Dong Lu Tunnel. *Tunnels and Metropolises, BalNema, Rotterdam,* pp. 1083-1088

Di Mariano, A., Gesto, J., Gens, A. & Schwarz, H. (2007) Ground deformation and mitigating measures associated with the excavation of a new Metro line. In *Proceedings of the Proc. XIV European Conference on Soil Mechanics and Geotechnical Engineering, ECSMGE*, pp. 1901-1906.

Frischmann, W., Hellings, J., Gittoes, G., Snowden, C. & DLR (1994) Protection of the mansion house against damage caused by ground movements due to the docklands light railway extension. *Proceedings of the Institution of Civil Engineers-Geotechnical Engineering,* **107** (2), pp. 65-76

Harris, D., Mair, R., Burland, J. & Standing, J. (1999) Compensation grouting to control tilt of Big Ben Clock Tower. *Geotechnical aspects of underground construction in soft ground,* pp. 225-232

Hejazi, Y., Dias, D. & Kastner, R. (2008) Impact of constitutive models on the numerical analysis of underground constructions. *Acta Geotechnica,* **3** (4), pp. 251-258

Katzenbach, R., Leppla, S., Vogler, M., Seip, M. & Kurze, S. (2013) Soil-structure-interaction of tunnels and superstructures during construction and service time. *Procedia Engineering,* **57** pp. 35-44

Ledesma Villalba, A. & Alonso Pérez de Agreda, E. (2017) Protecting sensitive constructions from tunnelling: the case of World Heritage buildings in Barcelona. *Géotechnique,* **67** (10), pp. 914-925

Mair, R., Harris, D., Love, J., Blakey, D. & Kettle, C. (1994) "*Compensation grouting to limit settlements during tunnelling at Waterloo Station, London*" *Tunnelling'94*, Springer, pp. 279-300.

Mair, R. & Taylor, R. (1996) *Geotechnical Aspects of Underground Construction in Soft Ground: Proceedings of the International Symposium on Geotechnical Aspects of Underground Construction in Soft Ground, London, UK, 15-17 April 1996.* AA Balkema.

Mair, R. & Taylor, R. (1997a) Theme lecture: Bored tunnelling in the urban environment. In *Proceedings of the Proceedings of the fourteenth international conference on soil mechanics and foundation engineering*, Rotterdam, pp. 2353-2385.

Mair, R. J. & Taylor, R. N. (1997b) Bored tunnelling in the urban environment. In *Proceedings of the Proceedings of 14th International Conference on Soil Mechanics and Foundation Engineering, London.* Vol. 4, pp. 2353-2385.

Metro, L. (2019), Vol. 2019 https://www.lisbon.net/metro [Accessed December 12, 2019]

Moitinho de Almeida, I. (2008) "*Guia de Telheiras* " Lisbon, pp. 4.

Nikiforova, N. & Vnukov, D. (2012) "*Geotechnical cut-off diaphragms for built-up area protection in urban underground development*" *Geotechnical Aspects of Underground Construction in Soft Ground*, CRC Press, pp. 945-950.

O'Reilly, M. & New, B. (1982) *Settlements above tunnels in the United Kingdom-their magnitude and prediction*. 090048862X.

Oteo, C., de la Fuente, P. & de Assis, S. (2007) Jet-grouting walls as protection to the buildings near urban tunnels. *Geotechnical Eng. in Urban Environments, Proc., 14th, ECSMGE*, **3** pp. 1504-1508

Peck, R. B. (1969) Deep excavations and tunneling in soft ground. *Proc. 7th ICSMFE, 1969*, pp. 225-290

Pedro, A. M. G. (2013) *Geotechnical Investigation Of Ivens Shaft In Lisbon*. PhD thesis. Imperial College London.

Potts, D. M., Zdravković, L., Addenbrooke, T. I., Higgins, K. G. & Kovačević, N. (2001) *Finite element analysis in geotechnical engineering: theory*. Thomas Telford London.

Quick, H., Michael, J. & Arslan, U. (2001) About the effect of preliminary measures on ground movements due to tunnelling. *Response of Building to Excavation-Induced Ground Movements, London*, **17** pp. 18

Rampello, S., Fantera, L. & Masini, L. (2019) Efficiency of embedded barriers to mitigate tunnelling effects. *Tunnelling and Underground Space Technology*, **89** pp. 109-124.

Simons, N. E. & Som, N. (1970) *Settlement of structures on clay: with particular emphasis on London clay*. Construction Industry Research and Information Association.

Society, B. T. (2004) *Tunnel lining design guide.* Thomas Telford.

Sola, P. R., Monroe, A. S., Martin, L., Blanco, M. A. & San Juan, R. (2003) "*Ground treatment for tunnel construction on the Madrid Metro*" *Grouting and Ground Treatment*, pp. 1518-1533.

Stallebrass, S. E. (1990) *Modelling the effect of recent stress history on the deformation of overconsolidated soils*. City University London.

Su, J. & Thomas, A. (2015) Design of sprayed concrete linings in soft ground—a Crossrail perspective. *Crossrail Project: Infrastructure design and construction*, **1** pp. 123-136

Telford, T. (2004) Tunnel lining design guide. *British Tunneling Society and the Institution of Civil Engineers*,

Viggiani, G. & Standing, J. (2001) "*26 The Treasury*" *Building response to tunnelling: Case studies from construction of the Jubilee Line Extension, London*, Thomas Telford Publishing, pp. 401-432.

Wan, M., Standing, J., Potts, D. & Burland, J. (2016) Measured short-term ground surface response to EPBM tunnelling in London Clay. *Géotechnique*, **67** (5), pp. 420-445

Yildizlar, B., Sayin, B., Karakas, A. S. & Akcay, C. (2014) Structural damage caused to RC buildings by tunnelling work.